40 Ar/ 39 Ar ages of Northwest Africa 7034 and Northwest Africa 7533

F. Lindsay, J. Delaney, C. Göpel, G. Herzog, R. Hewins, M. Humayun, K. Nagao, L. Nyquist, J. Park, J. Setera, et al.

The Meteoritical Society

Meteoritics & Planetary Science 56, Nr 3, 515–545 (2021)
doi: 10.1111/maps.13637

$^{40}Ar/^{39}Ar$ ages of Northwest Africa 7034 and Northwest Africa 7533

F. N. LINDSAY[1†], J. S. DELANEY[2], C. GÖPEL[3], G. F. HERZOG[1*], R. HEWINS[2,4], M. HUMAYUN[5], K. NAGAO[6,7], L. E. NYQUIST[8], J. PARK[1,6,9,10], J. B. SETERA[2,11], C.-Y. SHIH[12], C. C. SWISHER III[2], B. ZANDA[4,13], and B. D. TURRIN[2]

[1]Department of Chemistry & Chemical Biology, Rutgers University, New Brunswick, New Jersey 08854, USA
[2]Department of Earth & Planetary Sciences, Rutgers University, New Brunswick, New Jersey 08854, USA
[3]Institut de Physique du Globe, Sorbonne Paris Cité, University Paris Diderot, CNRS UMR 7154, F-75005 Paris, France
[4]Institut de Minéralogie, de Physique des Matériaux, et de Cosmochimie (IMPMC)—Sorbonne Université- Muséum National d'Histoire Naturelle, UPMC Université Paris 06, UMR CNRS 7590, IRD UMR 206, 61 rue Buffon, 75005 Paris, France
[5]Department of Earth, Ocean & Atmospheric Science, Florida State University, Tallahassee, Florida 32310, USA
[6]Division of Polar Earth-System Sciences, KOPRI (Korea Polar Research Institute), 26 Songdomirae-ro, Yeonsu-gu, Incheon 21990, Korea
[7]Geochemical Research Center, Graduate School of Science, University of Tokyo, 7-3-1 Bunkyo-ku, Tokyo 113 0033, Japan
[8]ARES, Code XI, NASA Johnson Space Center, Houston, Texas 77058, USA
[9]Department of Physical Sciences, Kingsborough Community College, Brooklyn, New York 11235, USA
[10]Department of Earth and Planetary Sciences, American Museum of Natural History, New York, New York 10024, USA
[11]Department of Earth and Atmospheric Sciences, Cornell University, Ithaca, New York 14853, USA
[12]216406 Locke Haven, Houston, Texas 77059, USA
[13]IMCCE, Observatoire de Paris—CNRS UMR 8028, 77 Av. Denfert Rochereau, 75014 Paris, France
*Corresponding author. E-mail: herzog@rutchem.rutgers.edu

(Received 14 January 2020; revision accepted 23 January 2021)

Abstract–The Martian breccias NWA 7034, NWA 7533, and paired meteorites record events ranging in age from 4.47 Ga to <200 Ma. Published ages indicate a period of major disturbance at ~1.4 Ga, examined in detail here through $^{40}Ar/^{39}Ar$ dating of handpicked grains and two small chips. Argon diffusion parameters were obtained for six samples. Also presented are He, Ne, Ar, Kr, and Xe contents of two small (<100 μg), handpicked mineral separates, a felsic "Light" sample and a mafic/pyroxene-rich "Dark" sample. The $^{40}Ar/^{39}Ar$ ages of five samples, four containing >1 wt% K and thought to be rich in feldspar and one containing <~1 wt% K, cluster near 1.4 Ga. The $^{40}Ar/^{39}Ar$ ages of nine grains with low K contents have a wide range of apparent ages from 0.3 ± 0.1 Ga to 2.9 ± 0.1 Ga for individual temperature steps, and from 0.74 ± 0.06 Ga to ~2.1 Ga for plateau ages. Isochron ages are less precise, but generally agree with plateau ages. Only two isochrons have the significantly positive intercepts expected in the presence of terrestrial or Martian atmospheric argon. At higher release temperatures, activation energies for diffusion obtained from ^{39}Ar data for six samples are generally 160–200 kJ mol^{-1}, consistent with published values for feldspathic minerals. For three of these samples, lower temperature data on Arrhenius plots are best fit with a much lower activation energy of <100 kJ mol^{-1}. We attribute the low values to the effects of varying degrees of shock on feldspathic minerals and/or the presence of phases in vitrophyric spherules produced by hydrothermal alteration. The low activation energies place an upper limit of ~14 ka on the terrestrial age of NWA 7034. Much lower concentrations of cosmogenic (c) ^{3}He and ^{21}Ne in the Light than in the Dark separate indicate substantial losses concurrent with or postdating cosmic ray irradiation. A one-stage, cosmic ray exposure (CRE) age for the Dark separate from NWA 7034 is estimated to be between 7 and 10 Ma from the concentrations of $^{3}He_c$ and

[†]Deceased June 14, 2017.

$^{38}Ar_c$, and of close to 15 Ma from the concentration of $^{21}Ne_c$. Most of the $^{40}Ar/^{39}Ar$ and noble gas data are compatible with (1) a heating and alteration event ~1.40 Ga caused by contact metamorphism, an impact, and/or the infiltration of hydrothermal fluids; and (2) at least one later event at lower temperatures that led to either loss of He and Ar from phases with low activation energies, or to gain of K. Most of the $^{40}Ar/^{39}Ar$ ages are consistent with the assembly of NWA 7034 1.4 Ga ago or perhaps earlier followed more recently by selective alteration. A more recent time of assembly is also consistent with these ages provided that the temperature stayed low. The five most precise $^{40}Ar/^{39}Ar$ ages of the samples analyzed are all ~1.4 Ga, a value seen frequently in other NWA 7034 chronometers and very similar to crystallization ages of nakhlites and chassignites (NC). Some CRE ages based on noble gases in NWA 7034 agree within their considerable uncertainties with those of NC. These two chronometric coincidences suggest that the NWA 7034 clan and the NC share a launch date on Mars. We propose that K-rich fluids derived from the nakhlite source area interacted with proto-NWA 7034 and modified the K/Ar ratios and ages of previously shocked feldspar grains, with the degree of modification depending on the degree of shock. The NWA 7034 clan may therefore be considered components from a metamorphic aureole around a nakhlite massif.

INTRODUCTION

Northwest Africa 7034 (NWA 7034) and paired meteorites are the first Martian polymict breccias found (Agee et al. 2013; Humayun et al. 2013; Hewins et al. 2017). Agee et al. (2013) inferred a planetary origin for the group from a relatively young $^{87}Rb/^{87}Sr$ age of 2.09 ± 0.08 Ga and a Martian origin from its oxygen isotope systematics and from geochemical and petrologic features shared with other Martian meteorites. Breccias record complex temporal sequences that may include crystallization ages of their clasts, a lithification age, and subsequent thermal disturbances. The spectrum of ages reported for NWA 7034 and pair NWA 7533 (see Table 1) includes Pb/Pb crystallization ages of >4.4 Ga and later disturbance ages of up to 1.4 Ga for zircons and apatites (Humayun et al. 2013; Bellucci et al. 2015; McCubbin et al. 2016; Bouvier et al. 2018; Costa et al. 2020), an Sm-Nd mineral isochron of 4.39 Ga (Nyquist et al. 2016), disturbed Rb-Sr isochrons of 1.7–3.8 Ga, Ar-Ar ages that range from 3.4 to 0.2 Ga, and U-Th-Sm-^{4}He ages indicating more recent losses of He (Cassata et al. 2018). Connecting each of these ages to specific events in the history of the breccia helps in understanding the processes that shaped the breccia.

Examined in detail, the distribution of these ages spreads over a few hundred Ma and raises questions about the number, nature, and extent of the resetting event or events. For example, in light of the large body of data confirming disturbances 1.5 Ga ago, McCubbin et al. (2016) concluded that "The 1.5 Ga age of NWA 7034 is likely a thermal event that coincides with rainout/breccia lithification." $^{40}Ar/^{39}Ar$ ages are generally more susceptible to disturbances than those based on Pb isotope systematics (with exceptions for metamictization). Cassata et al. (2018) reported an extensive study of the $^{40}Ar/^{39}Ar$ systematics in NWA 7034 samples. They concluded that "Collectively, the data suggest that metamorphism at 1500–1200 Ma is associated with protracted magmatic activity, and brecciation occurred much later (after ~225 Ma)." While this work was in the later stages of review, Costa et al. (2020) reported six concordant Pb/Pb ages between 200 and 1200 Ma for zircons extracted from NWA 7533. Costa and co-workers interpreted these ages as supporting lithification within the last 200 Ma.

We present a study of the $^{40}Ar/^{39}Ar$ ages of the Martian polymict breccia NWA 7034 and one of its paired stones, NWA 7533. The purpose of the work is to examine further the nature and timing of major events that affected the meteorite during the last 2 Ga. Using $^{40}Ar/^{39}Ar$ analyses of small samples, typically <~100 μg, and of single mineral grains, we set out to document in greater detail the history of NWA 7034, especially in the time period around 1.4 Ga BP. In standard $^{40}Ar/^{39}Ar$ dating, the stepwise heating of milligram samples yields results that average over the potassium concentrations, diffusion properties, and thermal histories of hundreds if not thousands of grains that may be diverse. The analysis of smaller samples can be useful in three ways. In the case of an uncomplicated, uniform sample, a foundation is laid for the interpretation of results from larger masses, albeit at the expense of extra effort and generally lower precision. In a more complex sample, for example, a breccia comprising diverse grains with different histories, the analysis of small samples may uncover

Table 1. Published radiometric ages (except $^{40}Ar/^{39}Ar$; see text) of NWA 7034 and paired meteorites.

NWA	Sample	Quantity	Method	Age (Ma)	Reference
7034	Bulk	950 mg	$^{146}Sm/^{142}Nd$ isochron, mineral separates	4475 ± 80	Nyquist et al. (2016)
	Bulk matrix	950 mg	$^{147}Sm/^{143}Nd$ isochron, mineral separates	4420 ± 70	
7034	Zircons, baddeleyite	5, 1 grains	U/Pb; SIMS	4439 ± 17(2σ)	Yin et al. (2014)
	Zircon		U/Pb; SIMS	4350 ± 13(2σ)	
	Zircon	5 μm	U/Pb; SIMS	Up: 4333 ± 38 Low: 1441 ± 37	
	Zircons	5 grains	U/Pb; SIMS	1410 ± 56(2σ)	
	Phosphates	5 μm	U/Pb; SIMS; $N = 150$)	1345 ± 47	
7533	Zircon rich phases from monzonitic melt rocks	10 grains	U/Pb SHRIMP ($N = 21$)	Up: 4430 ± 30 Low: 1720 ± 80	Humayun et al. (2013)
	Baddelyite	3 grains	U/Pb ($^{207}Pb/^{206}Pb$ only) Ion μprobe	>4300 ± 20	
7533	Plag; alk feld		Pb/Pb "Geochron"	Up: 4428 ± 28 Low: 1712 ± 85	Bellucci et al. (2015)
	Chlorapatite		U/Pb; SIMS ($N = 31$)	1357 ± 81(2σ)	
7034	Zircon (old)	6 grains	U/Pb; Ion μprob, SHRIMP	4431 ± 27	McCubbin et al. (2016)
	Zircon (young)	12 grains	U/Pb; Ion μprob, SHRIMP	1502 ± 98	
	Zircon (mixed)	10 grains	U/Pb; SHRIMP	Up: 4389 ± 44 Low: 739 ± 630	
	Baddeleyite	2 grains	Pb/Pb NanoSIMS	>4300 ± 80	
	(Cl-rich) apatite	17 grains	Pb/Pb; SHRIMP (T-W)	1495 ± 88	
7034	Zircons in igneous clasts	100 μm^2	U/Pb NanoSIMS	4424 to ~4460	Hu et al. (2019)
	Metamict zircons	2 grains		Up: 4465 ± 73	
	Apatites			Low: 1634 ± 93 1530 ± 65	
7034	Zircons	7 grains	U/Pb; TIMS	4476–4430	Bouvier et al. (2018)
7533	Ancient zircons, baddelyite	39, 2 grains 8 grains	U/Pb; TIMS	4331 to 4486 300 to 1548	Costa et al. (2020)
	Young zircons				
7034	Bulk	3 @ 0.5 g	subchondritic $^{187}Os/^{188}Os$	~1900, ~100, ~1500	Goderis et al. (2016)
7034	W	–	Rb/Sr	2190 ± 140	Agee et al. (2013)
7034	Bulk	69.7 mg	K/Ar	~1600; $^{40}Ar_{Tr} \equiv 0$	Cartwright et al. (2014)
	Bulk		U/He	170	
7906,7	Bulk	100 mg	K/Ar	<1270 ± 17	Stephenson et al. (2017)
			U/Th/He	180	

information otherwise lost or blurred. Finally, when the reliability of the results can be established, small samples optimize the scientific return obtainable when the available mass is limited.

Several questions pertinent to NWA 7034 seemed amenable to this approach. We look at how results for larger (>100 μg) and smaller samples compare; and at whether, and if so how, feldspathic minerals may differ with respect to their argon systematics. A broad scientific goal was to examine whether the variable ages of NWA 7034 samples (Table 1) record one extended or multiple periods of thermal activity on Mars. As an aid to interpreting the conditions on Mars that might have influenced the $^{40}Ar/^{39}Ar$ ages, we determined the Ar diffusion parameters of six of the samples by using a method described by Setera et al. (2020).

The noble gas contents of NWA 7034 are of interest in the characterization of its cosmic ray exposure (CRE) age (Cartwright et al. 2014; Stephenson et al. 2017; Cassata et al. 2018). Published studies present single-stage exposure ages ranging from ~5 Ma (Cartwright et al. 2014; Stephenson et al. 2017) to >8 Ma (Busemann et al. 2015; Cassata et al. 2018). Noble gas data collected as part of this study are used to reassess the CRE age.

SAMPLING AND EXPERIMENTAL METHODS

Samples from NWA 7034

We analyzed the argon in two groups of samples from NWA 7034. The first group was prepared at the

Johnson Space Center from material supplied by the Institute of Meteoritics at the University of New Mexico (Nyquist et al. 2016). After crushing and sieving, magnetic separation of the 100–200 mesh size fraction at a current of 0.5 A yielded a small, nonmagnetic portion composed of ~40 clear grains with a total mass of ~120 μg. This material was taken for $^{40}Ar/^{39}Ar$ analysis. The complementary magnetic portion, which contained most of the pyroxene and plagioclase in the original sample, was further separated using heavy liquids. Nyquist et al. (2016) present chronometric and compositional results for these density separates. We assume that the two plagioclase separates from NWA 7034—the "nonmagnetic" one of ~120 μg, which was the source of our samples 22220, 22221, and 22222, and the feldspathic material later separated from the "magnetic" fraction and analyzed by Nyquist et al. (2016)—have similar histories in the meteorite, so that comparisons of ages obtained from them will be unbiased.

A second group of six samples from NWA 7034 (22344, 22345, 22346, 22348, 22349, and 22350) was extracted from several chips kindly provided by C. Agee at the University of New Mexico (UNM). We polished them, identified individual clasts optically, and mined some of those clasts with hand tools for lithic components. Although most of the grains obtained were too small (<1 μg) to analyze individually for argon isotopes, we retained petrologic context by keeping grains from discrete clasts together in most cases.

The sample T20 (from Chip 5; 22344) was part of a large (1.75 mm × 0.75 mm) crystal that fell apart during excavation (Fig. 1). The sample 22345 consisted of eight grains from the matrix of Chip 2. No effort was made to separate individual minerals from the sample 22346, but this small (11.5 μg) collection of crumbs from Chip 4 had a light color and thus seemed be rich in feldspar, an impression confirmed by other analyses (see below). 22348, the most massive sample analyzed (202 μg), came from Chip 7, was untreated, and was intended to represent the "bulk" meteorite. The sample from chip 6 (22350) was made up of six grains taken from within a discrete clast that disaggregated during excavation. 22349 (6 μg) was a collection of feldspathic grains taken from several different clasts.

In addition, a small mass of NWA 7034 from the chips provided by Carl Agee was ground, sieved (>75 μm), and separated (sink/float) into two fractions with a solution of heavy liquid LST (lithium polytungstate) with a density 2.85 g cm^{-3}. From the denser split, we handpicked ~64 μg of dark crystals, determined by EDX (energy-dispersive X-ray analysis) at Rutgers University to be enriched in pyroxene, and from the less dense split, 22 μg of white or transparent crystals, also determined by EDX to be enriched in feldspar. Both samples were taken for noble gas analyses at the University of Tokyo. We will refer to these samples as Dark and Light, respectively.

Samples from NWA 7533

The grains of NWA 7533 were separated at the Institut de Physique du Globe. A sample of 1.4 g was gently crushed in a sapphire mortar, passed through nylon sieves, and washed with pure ethanol to remove fine dust. Light-colored grains were handpicked with tweezers with Teflon-covered tips. Scanning electron microscopy of several grains chosen at random from this separate (Ref.) showed that the plagioclases were transparent whereas the K-feldspars were milky white. For this work, we selected the largest grains available.

EDX Analysis and Sample Selection

Separated grains from both NWA 7034 and NWA 7533 were mounted on 1 inch carbon rounds. Energy-dispersive (X-ray) spectroscopy (EDX) was carried out by using a JEOL JXA 8200 electron microprobe at the Rutgers University Micro-analytical Laboratory. The electron excitation voltage was 15 kV, the beam current 20 nA, and the spot size ~1 μm. The final selection of grains for $^{40}Ar/^{39}Ar$ analyses was based on the K concentrations measured by EDX and compositional and visual evidence for the predominance of a single mineral.

Neutron Irradiation, Age Standards, and Ar Isotopic Analysis

The NWA 7034 and 7533 samples along with the reference minerals were loaded into pits drilled into 1 cm diameter Al-disks for neutron irradiation. The pits are arranged in a controlled geometry to facilitate the correction of any measurable gradients in the neutron flux. The samples were irradiated in two batches (#66, 79.8 h; and #68, 81 h), neither of them Cd-shielded, at the US Geological Survey TRIGA reactor in Denver, Colorado.

Our primary age standard for both irradiations was Fish Canyon (FC-2) sanidine (t_{FC} = 28.201 Ma; Kuiper et al. 2008). Values of J ranged from 0.01902 to 0.01912 and from 0.01938 to 0.01970 for the samples of irradiation #66 and of irradiation #68, respectively.

In irradiation #68, we included Hb3gr (t_{Hb3gr} = 1083 Ma; Blackburn et al. 2017) as a secondary age standard. To assess the internal consistency of our results for the two age standards with published work, we compared the experimentally

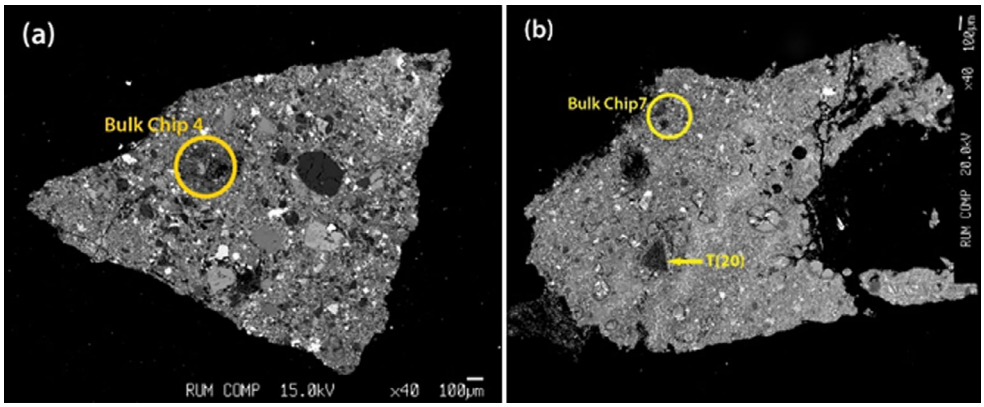

Fig. 1. Backscattered electron images. a) Chip 4, showing the location of sample 22346. b) mosaic of Chip 7 showing the location of clast T20 (22344) and bulk chip 7 (22348) prior to sampling. (Color figure can be viewed at wileyonlinelibrary.com.)

measured quantity $\frac{^{40}Ar^*_{Hb3gr}}{^{39}Ar_{Hb3gr}} / \frac{^{40}Ar^*_{FC}}{^{39}Ar_{FC}} \equiv \Delta R^{Hb3gr}_{FC}$ with the value of $\frac{e^{\lambda_{Total} t_{Hb3gr}} - 1}{e^{\lambda_{Total} t_{FC}} - 1}$ calculated from the independently determined U-Pb ages (see Renne et al. 2010); λ_{Total} is the total ^{40}K decay constant. Our measured value of ΔR^{Hb3gr}_{FC} is 52.20 ± 0.17 ($\pm 0.3\%$). The value of the expression calculated from the U-Pb age of FC (28.2 Ma) from the same unit (Wotzlaw et al. 2013) and the U-Pb titanite age of 1083 Ma from the Lone Grove Pluton (Hb3gr) is 52.21 using λ_{Total} from Steiger and Jäger (1977). With λ_{Total} from Renne et al. (2011), we find $R_{Hb3gr} = 52.17$. These results show that the ages presented here may be compared directly to ages referred to age standards other than Fish Canyon.

As a rule and in this study, the uncertainty of the measured age of a sample depends primarily on the relative uncertainty of the ^{39}Ar measurements for that sample. For this reason, the use of an age standard older than Fish Canyon sanidine is not expected to have much effect on the precision of sample ages. Indeed, the use of our Hb3gr results (instead of those for FC) to calculate J values and ages increases Δt_{Sample} slightly. The poorer performance of Hb3gr can be traced to its lower (compared to FC) K content and hence larger value of $\frac{\delta^{39}Ar_{Std}}{^{39}Ar_{Std}}$.

Argon isotope measurements were conducted at Rutgers University on an upgraded mass analyzer products (MAP) 215–50 noble gas mass spectrometer following procedures given in Turrin et al. (2010) and Setera et al. (2020). Samples with RUIDs <22244 were heated directly with a New Wave, 40 W CO_2 laser at increasing power settings, but without temperature measurement. Samples 22344–22350 were heated indirectly on Ta platforms as summarized by Setera et al. (2020) with temperatures measured pyrometrically.

For indirect heating, each grain was placed in a dimple ~1 mm in diameter and ~200 µm deep impressed in a 5×5 mm square cut from high-purity Ta foil 0.008 mm thick. The corners of the square were folded downward at 90° to make supporting legs that reduced heat losses to the chamber. Temperatures were measured, but not controlled, with a Mikron-M780 two-color pyrometer with a 1 µm spectral range. An instrumental adjustment available in the pyrometer allows corrections for the emissivity of Ta. We confirmed the reliability of this adjustment and the uniformity of temperature across the platform by simultaneously observing the melting, and measuring the melting temperatures of Sn, Al, Cu, Au, and Pyrex. The melting temperatures (in °C) agreed with accepted values to within 0.3%; the manufacturer specifies a pyrometer accuracy of 0.5%. The minimum temperature measurable is ~500 °C. For lower temperatures, we extrapolated an empirical correlation between temperature and laser power; uncertainties in this region are larger, perhaps 1%. Setera et al. (2020) describe the details.

Typical blanks (10^{-18} mol) were ^{40}Ar, <110; ^{39}Ar, 3.8; ^{38}Ar, 1.1; ^{37}Ar, 23; and ^{36}Ar, 3.8. The blanks were independent of the laser power applied.

For all of the ages presented, uncertainties are expressed as 1σ unless otherwise specified, and we use the following symbols and constants: Ar* = radiogenic argon; $^{39}Ar_K = ^{39}Ar$ produced from ^{39}K; $^{37}Ar_{Ca} = ^{37}Ar$ produced from ^{40}Ca; $\lambda_\epsilon = 5.81 \times 10^{-11}$ yr^{-1}; $\lambda_{(\epsilon+\beta)} = 4.962 \times 10^{-10}$ yr^{-1}; $^{40}K/K_{total} = 1.167 \times 10^{-4}$ (Steiger and Jäger 1977); $^{36}Ar_{Ca}/^{37}Ar_{Ca} = (2.57 \pm 0.03) \times 10^{-4}$; $^{39}Ar_{Ca}/^{37}Ar_{Ca} = (6.62 \pm 0.1) \times 10^{-4}$; $^{40}Ar_K/^{39}Ar_K = (9.8 \pm 0.2) \times 10^{-3}$; $^{38}Ar_K/^{39}Ar_K = (1.319 \pm 0.001) \times 10^{-2}$.

Data were processed with the software Mass Spec Version 7.816, from Alan Deino at the University of California, Berkeley.

Noble Gas Analysis of Unirradiated Light and Dark

The elemental concentrations and the isotopic compositions of He, Ne, Ar, Kr, and Xe were analyzed using a noble gas mass spectrometer (modified-VG5400/MS-II) at the Geochemical Research 165 Center, University of Tokyo (Nagao et al. 1996). The mass spectrometer was connected to a glass sample holder via a noble gas extraction line equipped with (1) a molybdenum crucible mounted in an extraction furnace; (2) a gas purification line; and (3) for system calibration, a canister containing known amounts of air, ^{3}He, and ^{4}He and accessible via a gas pipette (e.g., Okazaki and Nagao 2004; Nagao et al. 2008). The gas purification line was separately heated to about 250 °C for 1 day to attain ultra-high vacuum. The samples were wrapped in Al foil (10 μm thick) and loaded in a glass sample holder connected to the extraction furnace. The samples were heated under ultra-high vacuum to 150 °C to eliminate adsorbed terrestrial atmospheric noble gas contamination. The molybdenum crucible in the extraction furnace was degassed repeatedly at 1900 °C to lower the extraction blank. As the Light and the Dark samples had low masses and low noble gas concentrations, extractions were carried out in one total melting step.

The gases were purified using two Ti-Zr getters heated at about 750 °C and SAES-getters (NP-10). He and Ne were separated by trapping Ar, Kr, and Xe on charcoal at −196 °C. During the measurement of neon isotopes, two additional, similar traps removed ^{40}Ar and CO_2. The corrections for $^{40}Ar^{2+}$ and for $^{12}C^{16}O_2{}^{2+}$ to the ion beam intensities of ^{20}Ne and ^{22}Ne were <5% and 1%, respectively. After He and Ne analysis, Ar, Kr, and Xe were desorbed from the charcoal trap and separated from each other cryogenically at temperatures of −173, −123, and −43 °C for Ar, Kr, and Xe, respectively.

Mass discrimination correction factors and sensitivities for all noble gases except He were determined by analyzing a known amount of air (~5×10^{-4} cm^{3}STP). The mass discrimination for ^{3}He/^{4}He was determined using a ^{3}He–^{4}He mixture with ^{3}He/^{4}He = 1.71×10^{-4}. Blank corrections were applied to all noble gas data. The experimental errors for isotope ratios given are 1-σ. The uncertainty of concentrations that will be shown in Table 3 is estimated to be about 10% in each temperature step.

RESULTS

Compositional analyses by EDX are provided in Table 2. Noble gas data for Light and Dark fractions of NWA 7034 are given in Table 3. Cosmogenic noble gas abundances and CRE ages are given in Table 4, which also summarizes CRE ages from the literature. Ar-Ar results are given in Table A2.1 in supporting information. Plateau ages are given in Table 5 and isochron ages in Table 6. Plateau and isochron plots for these data are shown in Fig. A3.1 in supporting information.

As expected, the texture of our NWA 7034 sample shows characteristics of an impact-produced breccia (Figs. 1 and 2). The likelihood of terrestrial alteration by a fluid phase is indicated by calcite veining in several plagioclase grains that crosscut the adjacent breccia (see also Wittmann et al. 2014; Hewins et al. 2017). Petrographic evidence for fluid alteration on Mars has been discussed by Agee et al. (2013), Lorand et al. (2015, 2018), Liu et al. (2016), McCubbin et al. (2016), MacArthur et al. (2019), Hu et al. (2019), Guitreau and Flahaut (2019), and Humayun et al. (2019).

EDX Analyses of Grains Selected for ^{40}Ar/^{39}Ar Analysis

We made at least one semiquantitative EDX spot analysis for 13 of the 16 samples analyzed for Ar. Not probed were the grains in 22346 and 22348 although we did analyze random spots from nearby material on the parent chips, 4 and 7, respectively. Also not probed was sample 22349, which consisted of bits of feldspar from all chips.

Our semiquantitative EDX analyses of unmounted and unpolished grains were intended for a preliminary grouping of the samples by K concentration. Later, ^{40}Ar/^{39}Ar analyses gave independent measures of the K concentrations. Although the quantitative agreement of results of the two methods for K was generally poor, for 11 of the 13 samples, the ^{40}Ar/^{39}Ar results confirmed the EDX identification of low-K (<1 wt%) and high-K (>1 wt%) grains. We use the umbrella terms "plagioclase" for the low-K grains and "alkali feldspar" for the high-K grains with the caution that these grains may not be monomineralic, that is, that "plagioclase" may contain other light-colored, nonmagnetic phases such as chlorapatite, and that "alkali feldspar" may contain other K-bearing phases.

For six of the seven NWA 7533 samples, low K contents are consistent with the visual identification of the clear grains as plagioclase. In two samples, 22242 (NWA 7533) and 22345 (NWA 7034), the disagreement between the independently measured K contents prevented an unambiguous, high-K/low-K assignment. We base our characterization of 22242 and 22345 as "plagioclase" on both the appearance of the grains (see above) and the low levels of K obtained from the Ar measurements, rather than on the much higher levels determined in the EDX spot analyses, which are subject to surface artifacts and probe only small portions of the grain surfaces. The ^{40}Ar/^{39}Ar measurements, in contrast, probe the entire sample.

Table 2. Elemental composition of NWA 7034 and pairing group samples.

	Bulk		Plag rich				Pyx rich		
Element	Ref. 1	Ref. 2	22348	Chip 7	Ar/Ar*	Light	22348	Chip 7	Dark
O	41.18	43.68	46.79	46.83	46.79	48.35	43.20	43.27	44.14
Na	2.77 ± 0.39	2.08 ± 0.02	4.6 ± 1.3	4.8 ± 1.4	2.8 ± 1.8	3.5 ± 1.2	0.04 ± 0.01	0.04 ± 0.02	2.6 ± 0.9
Mg	4.71 ± 1.01	6.57 ± 0.12	0.02 ± 0.03	0.03 ± 0.04	0.18 ± 0.13	0.61 ± 0.33	14.4 ± 1.1	14.4 ± 0.9	5.5 ± 3.8
Al	5.93 ± 0.83	5.66 ± 0.03	14.46 ± 1.04	14.2 ± 1.2	15.0 ± 2.7	14.1 ± 2.9	1.06 ± 0.82	1.0 ± 0.8	10.0 ± 3.4
Si	22.23 ± 0.85	22.58 ± 0.14	26.66 ± 1.34	27.1 ± 1.8	24.3 ± 2.0	24.3 ± 1.3	24.8 ± 0.8	24.8 ± 0.8	21.4 ± 3.4
P	0.33 ± 0.09	0.56 ± 0.02				0.28 ± 0.13			0.42 ± 0.31
S	0.04 ± 0.08	0.03 ± 0.01							
K	0.28 ± 0.05	0.39 ± 0.02	0.33 ± 0.16	0.37 ± 0.21	5.8 ± 8.1	1.8 ± 3.2	0.02 ± 0.02	0.04 ± 0.02	0.8 ± 1.0
Ca	6.38 ± 0.91	5.03 ± 0.10	6.64 ± 1.71	6.2 ± 2.0	4.8 ± 3.7	6.5 ± 2.9	1.02 ± 0.37	1.1 ± 0.4	5.9 ± 3.5
Ti	0.59 ± 0.13	0.61 ± 0.02	0.02 ± 0.01	0.02 ± 0.01	0.03 ± 0.04	0.20 ± 0.36	0.17 ± 0.10		0.3 ± 0.3
Cr	0.00 ± 0.00	0.18 ± 0.01	0.01 ± 0.01	0.02 ± 0.01		0.06 ± 0.09	0.16 ± 0.14	0.2 ± 0.1	0.1 ± 0.1
Mn	0.22 ± 0.04	0.28 ± 0.02	0.01 ± 0.01	0.01 ± 0.01	0.03 ± 0.03	0.05 ± 0.09	0.49 ± 0.10	0.5 ± 0.1	0.3 ± 0.2
Fe	10.11 ± 1.92	12.90 ± 0.23	0.45 ± 0.22	0.43 ± 0.21	0.28 ± 0.22	0.57 ± 0.49	14.7 ± 1.8	14.7 ± 1.6	9.1 ± 8.4
Sm	6.43 ± 0.06	3.76 ± 0.08							
Th	2.64 ± 0.06	0.99 ± 0.04							
U	0.51 ± 0.02	0.29 ± 0.03							
~No. spots			12	12	16	12	6	7	20

All elements in wt% except Sm, Th, U (ppm wt). Oxygen by difference. All results except (Ref. 1) and (Ref. 2) are from this work by EDX; see text.

Ref. 1 = Agee et al. (2013). Ref. 2 = Wittmann et al. (2015); includes pairs.

*Data for samples that were taken for $^{40}Ar/^{39}Ar$ dating and had K < 1 wt%.

EDX Analyses and Elemental Composition of Unirradiated Light and Dark Separates

For both the Dark and the Light separates, we chose ~20 EDX spot analyses that appear to be the most reliable based on phase stoichiometry. Average values are shown in Table 2. Low but finite Mg and Fe contents indicate that Light contained small fractions of pyroxene and iron oxides; a phosphorus elemental concentration of 0.3 wt% suggests the presence of apatite. The Dark sample contains much more Mg and Fe than does the Light sample, as would be expected for pyroxene-rich material, but Dark also has two-thirds of Light's concentrations of Al and Na, both of which signal the presence of feldspathic minerals. The apparent concentration of phosphorus is about the same in Light and Dark. The diverse nature of the grains in the mineral separates is reflected in the large standard deviations of the major element means.

Noble Gases in Unirradiated Light and Dark Separates

The results from the noble gas analyses of the mineral separates are presented in Table 3. The isotopic ratios indicate large fractions of noncosmogenic ("trapped") Kr and Xe in both Light and Dark and of noncosmogenic Ar in Light. Large uncertainties of the isotopic ratios for Kr and Xe preclude identification of the trapped component as Q, solar wind, terrestrial atmosphere, or fractionated terrestrial atmosphere. The absolute concentrations of ^{40}Ar (10^{-6} cm^3 STP g^{-1}), 262 and 79 in Light and Dark, respectively, however, suggest that the trapped Kr and Xe are terrestrial. In particular, the Light separate contains considerably more ^{40}Ar (262; Table 3) than all but 3 of the 16 samples subjected to $^{40}Ar/^{39}Ar$ analysis (range 6–603; median 27; Table A2.1 in supporting information). Similarly, the Dark separate contains more ^{40}Ar (79) than the values reported for bulk unirradiated samples (27, Cartwright et al. 2014; 20, Stephenson et al. 2017). While the $^{36}Ar/^{38}Ar$ ratios of Light and Dark, 5 and 3.7, also are consistent with the presence of air Ar, they do not require it. It seems likely, therefore, that Light and Dark adsorbed Kr and Xe along with Ar from the terrestrial atmosphere. As shown below, the presence of atmospheric ^{40}Ar helps make sense of the K/Ar ages of the separates, while the presence of solar or Martian atmospheric ^{40}Ar does not.

Cosmic Ray Exposure Ages for Unirradiated Light and Dark Separates

The concentrations of cosmogenic ^3He, ^{21}Ne, and ^{38}Ar along with the formulas used and assumptions made in calculating them are presented in Table 4 and Appendix S1 in supporting information. If interpreted

Table 3. Noble gas contents of Light (22 μg) and Dark (64 μg) separates handpicked from NWA 7034.

	^{3}He	^{4}He		^{20}Ne	^{21}Ne	^{22}Ne			^{36}Ar	^{38}Ar	^{40}Ar		
	10^{-9} cm^3 g^{-1}	10^{-6} cm^3 g^{-1}	^{3}He/^{4}He	10^{-9} cm^3 g^{-1}			^{20}Ne/^{22}Ne	^{21}Ne/^{22}Ne	10^{-9} cm^3 g^{-1}		10^{-6} cm^3 g^{-1}	^{38}Ar/^{36}Ar	^{40}Ar/^{36}Ar
Light	8.2 ± 7.1	1.18 ± 0.50	0.007 ± 0.005	62.1 ± 23.1	4.8 ± 1.4	13.9 ± 2.6	4.5 ± 0.8	0.37 ± 0.03	599 ± 75	119 ± 15	262 ± 33	0.199 ± 0.003	438 ± 11
Dark	132 ± 14	40.7 ± 4.2	0.002 ± 0.000	62.08 ± 12.59	46.68 ± 5.06	61.32 ± 6.50	1.01 ± 0.06	0.76 ± 0.00	159 ± 21.07	42.77 ± 5.77	79 ± 10	0.268 ± 0.007	494 ± 18

	^{84}Kr 10^{-9}cm^3 g^{-1}	^{78}Kr/^{84}Kr	^{80}Kr/^{84}Kr	^{82}Kr/^{84}Kr	^{83}Kr/^{84}Kr	^{86}Kr/^{84}Kr
Light	4.39 ± 0.09	0.0065 ± 0.0040	0.037 ± 0.013	0.200 ± 0.050	0.210 ± 0.041	0.335 ± 0.044
Dark	1.6 ± 0.03	0.0098 ± 0.0046	0.061 ± 0.013	0.247 ± 0.036	0.225 ± 0.036	0.320 ± 0.032

	^{132}Xe 10^{-9} cm^3 g^{-1}	^{124}Xe/^{132}Xe	^{126}Xe/^{132}Xe	^{128}Xe/^{132}Xe	^{129}Xe/^{132}Xe	^{130}Xe/^{132}Xe	^{131}Xe/^{132}Xe	^{134}Xe/^{132}Xe	^{136}Xe/^{132}Xe
Light	0.48 ± 0.03	0.005 ± 0.026	0.010 ± 0.016	0.080 ± 0.059	1.21 ± 0.35	0.172 ± 0.086	0.99 ± 0.38	0.40 ± 0.16	0.25 ± 0.17
Dark	0.20 ± 0.01	0.014 ± 0.019	0.015 ± 0.020	0.104 ± 0.070	1.20 ± 0.35	0.174 ± 0.094	0.83 ± 0.24	0.48 ± 0.20	0.35 ± 0.13

Blanks (10^{-12} cm^3 STP): ^{4}He, 63; ^{20}Ne, 2.2; ^{22}Ne, 0.23; ^{36}Ar, 2.9; ^{40}Ar, 865; ^{84}Kr, 0.096; ^{130}Xe, 0.005; ^{132}Xe, 0.038. Blanks for other isotopes were estimated by assuming the terrestrial isotopic ratios for each element. To convert from cm^3 g^{-1} to mol g^{-1}, multiply by 4.464×10^{-5}.

Table 4. Cosmic ray exposure ages based on ^{3}He, ^{21}Ne, and ^{38}Ar.

Sample	$^{3}He_c$[a] 10^{-8} cm^3 STP g^{-1}	$^{21}Ne_c$[b]	$^{38}Ar_c$[c]	$(^{22}Ne/^{21}Ne)_c$	P_3 10^{-8} cm^3 STP g	P_{21}	P_{38} g-Ma^{-1}	Remarks[d]	t_3 Ma[e]	t_{21}	t_{38}
Literature values											
NWA 7034[1]	8.2 ± 0.1	1.78 ± 0.03	0.74 ± 0.08	1.27 ± 0.02	1.71	0.238	0.122	LM R10 d10 to R25 d25	4.8 ± 0.4	7.5 ± 1.5	6.1 ± 1.3
					1.49	0.262	0.155	LM R85 d85	5.5 ± 0.5	6.8 ± 1.4	4.8 ± 0.5
					1.61	0.156	0.138	EM	5.1 ± 0.4	11.4 ± 2.3	5.4 ± 0.6
						0.198		EM + P_{21}(Na)[1]		9.0 ± 1.8	
NWA 7906[2]	6.7 ± 0.1	1.65 ± 0.01	0.22 ± 0.03	1.21 ± 0.01	1.58	0.249	0.158	LM R85 d85; Na = 1.5 wt%	4.3 ± 0.4	6.6 ± 0.7	1.4 ± 0.1
NWA 7907[2]	5.8 ± 0.1	1.60 ± 0.01	0.44 ± 0.04	1.20 ± 0.09	1.59	0.261	0.169	LM R85 d85; Na = 1.5 wt%	3.7 ± 0.4	6.1 ± 0.6	2.6 ± 0.3
NWA 7034[3]	3.61	0.98	0.511	1.222	1.69	0.237	0.107	EM	2.1 ± 0.3	4.1 ± 0.5	4.8 ± 0.5
					0.47	0.110	0.083	LM R120 d115	7.7 ± 0.8	8.9 ± 0.9	9.6 ± 1.0
					1.71	0.238	0.122	LM R10 d10 to R25 d25	1.91	4.10	4.18
NWA 8114[4]										8.2	8.2
This work											
NWA 7034 Light	0.8 ± 0.7	0.46 ± 0.14	0.80 ± 0.10	1.33 ± 0.24	1.66	0.31	0.22	LM R25 d1; SCR + GCR[5]	0.5 ± 0.4	1.5 ± 0.4	3.6 ± 0.5
					1.83	0.29	0.22	LM R25 d10	0.4 ± 0.4	1.6 ± 0.5	3.6 ± 0.5
					1.52	0.27	0.25	LM R85 d85	0.5 ± 0.5	1.7 ± 0.5	3.2 ± 0.4
					0.81	0.14	0.15	LM R120 d115	1.0 ± 0.9	3.3 ± 1.0	5.3 ± 0.7
					0.92	0.14	0.11	LM R500 d0-4	0.9 ± 0.8	3.4 ± 1.0	7.1 ± 0.9
					1.72	0.24	0.17	EM + P_{21}(Na)[6,7]	0.5 ± 0.4	1.9 ± 0.6	4.7 ± 0.6
					1.67	0.20	0.17	EM + P_{21}(Na)[6,8]	0.5 ± 0.4	2.3 ± 0.7	4.7 ± 0.6
NWA 7034 Dark	13.2 ± 1.4	4.66 ± 0.51	1.49 ± 0.21	1.28 ± 0.01	1.66	0.31	0.18	LM R25 d1; SCR + GCR[5]	8.0 ± 0.8	15.2 ± 1.7	8.3 ± 1.2
					1.83	0.30	0.157	LM R25 d10	7.2 ± 0.8	15.3 ± 1.7	9.5 ± 1.3
					1.49	0.29	0.171	LM R85 d85	8.9 ± 0.9	15.9 ± 1.7	8.7 ± 1.2
					0.79	0.16	0.103	LM R120 d115	16.8 ± 1.7	29.7 ± 3.2	14.4 ± 2.0
					0.92	0.15	0.080	LM R500 d0 to 4	14.3 ± 1.5	31.9 ± 3.5	18.5 ± 2.6
					1.72	0.27	0.14	EM + P_{21}(Na)[6,7]	7.7 ± 0.8	17.2 ± 1.9	10.6 ± 1.5
					1.67	0.22	0.14	EM + P_{21}[6,8]	7.9 ± 0.8	20.9 ± 2.3	10.6 ± 1.5

Subscript "c" = cosmogenic; subscript "Tr" = trapped. In the formulas of notes a–d, an isotope without a subscript refers to the measured value.

References: 1) Cartwright et al. (2014). 2) Stephenson et al. (2017). 3) Cassata et al. (2018). 4) Busemann et al. (2015) quote a "mean (^{21}Ne,^{38}Ar) age." 5) SCR from Roth et al. (2017); rigidity, R_0 = 100 MV. 6) $P_{21}(Na) = 1.1 \times P_{21}(Mg)$. 7) $(^{22}Ne/^{21}Ne)_c \equiv 1.27$. 8) $(^{22}Ne/^{21}Ne)_c \equiv 1.16$. Age calculations are based on gas contents as measured with no adjustment to the values for Dark.

[a] $^{3}He_c = {}^{3}He$.

[b] $^{22}Ne_c = \frac{R_{Tr}{}^{22}Ne - {}^{20}Ne}{R_{Tr} - R_c}$; $^{21}Ne_c = {}^{21}Ne + \frac{r_{Tr}R_c}{R_{Tr} - R_c}{}^{22}Ne - \frac{r_{Tr}}{R_{Tr} - R_c}{}^{20}Ne$; $R_{Tr} = (^{20}Ne/^{22}Ne)_{Tr} = 7.3$ (Nyquist et al. 2015). The use of $R_{Tr} = 9.8$ (e.g., Swindle et al. 1986) has a negligible effect on the value of $^{21}Ne_c$ and on $(^{22}Ne/^{21}Ne)_c$ of Dark but gives an implausibly large value for $(^{22}Ne/^{21}Ne)_c$ of Light. $R_c = (^{20}Ne/^{22}Ne)_c = 0.82$; $r_{Tr} = (^{21}Ne/^{22}Ne)_{Tr} = 0.029$.

[c] $^{38}Ar_c = \frac{R_{Tr\text{-}Ar}{}^{38}Ar - {}^{36}Ar}{R_{Tr-Ar} - R_{c\text{-}Ar}}$; $R_{Tr\text{-}Ar} = (^{36}Ar/^{38}Ar)_{Tr} = 5.35$, $R_{c\text{-}Ar} = (^{36}Ar/^{38}Ar)_c = 0.65$ (Herzog and Caffee 2014; Wieler et al. 2016).

[d] LM = Leya and Masarik (2009). EM = Eugster and Michel (1995). R = radius in cm; d = depth in cm.

[e] Uncertainties based on uncertainty of cosmogenic ^{3}He, ^{21}Ne, or ^{38}Ar only.

Table 5. Integrated and plateau ages (Ma) of NWA 7533 and NWA 7034 samples.

RUID	Mass (μg)	Desc.	# part.	K (wt%)	Integ. Age	±	Min. age (step)	±	Plat. age CL 90	±	%^{39}Ar	Plat. age CL 95	±	%^{39}Ar
NWA 7533														
22219	21	plag + ap	1	0.13	2306	15	1503(B)	76	No plateau			No plateau		
22239	16	plag	4	0.27	1066	8	708(E)	14	747	6	67	No plateau		
22240	33	plag	9	0.19	1973	9	1438(B)	10	No plateau			No plateau		
22241	11	plag	4	0.41	1464	10	1401(B)	11	1411	8	74	1411	8	74
22242	2	plag	1	0.18	740	55	310(B)	100	785	50	65	No plateau		
22243	21	plag	11	0.15	1921	16	1520(B)	24	No plateau			No plateau		
22244	4	alk fsp	1	7.95	1324	5	1030(A)	4	1361	3	85	1361	3	85
NWA 7034														
22220	16	plag	6	0.10	1890	120	1485(B)	55	2145	92	60	2145	92	60
22221	6	alk fsp	1	2.92	1412	12	*1241(F)*	*92*	1413	8	100	1413	8	100
22222	21	plag	12	0.17	1585	40	1225(A)	44	1620	38	55	1620	38	55
22344	37	alk fsp + ap	1	2.78	1665	5	1287(F)	7	No plateau			No plateau		
22345	20	plag	8	0.18	2073	40	1450(I)	322	2233	28	63	No plateau		
22349	6	alk fsp + ap	several	1.86	1451	13	1377(C)*	20	1416	10	84	No plateau		
22350	5.5	alk fsp	6	1.32	1480	13	921(C)	65	1432	9	80	1436	9	60
22346	11.5	bulk	chip	0.57	1480	29	1218(D)	87	1376	20	99	1353	23	75
22348	202	bulk	chip	0.27	1155	3	723(A)	25	1284	3	52	1284	3	52

Desc. = approximate mineralogical description based primarily on light color, K content, and the detection of phosphorus by EDX; plag = plagioclase (<1 wt% alk fsp = alkali feldspar (>1 wt%); ap = apatite; # part. = number of particles taken for Ar/Ar analysis; K [wt%] from ^{39}Ar assuming K = 10.0 wt% in Fish Canyon sanidine (Dazé et al. 2003); Integ. age = integrated age; Plat. age = plateau age; %^{39}Ar = fraction of ^{39}Ar in plateau; CL = confidence limit.

*Step J (629 ± 252 Ma) is an outlier.

in terms of a one-stage irradiation that took place during transit to Earth, our results tend to support a CRE age older than 5 Ma as favored by Busemann et al. (2015) and by Cassata et al. (2018) (Table 4). The results also show appreciable losses of noble gases from feldspathic phases. If such losses are common in NWA 7034, their consideration should be part of the interpretation of results for bulk samples. We discuss details in Appendix S1 and present our main observations here.

For any given set of assumed shielding conditions, the CRE ages of Light are younger than those of Dark: T_3(Light)/T_3(Dark) ~ 0.05; T_{21}(Light)/T_{21}(Dark) ~ 0.10; T_{38}(Light)/T_{38}(Dark) ~ 0.4. We infer that Light lost at least 90% of its cosmogenic ^{3}He and >50% of its cosmogenic ^{21}Ne. If these systematic differences apply generally, then reported values of T_3 and T_{21} for bulk samples are lower limits.

The large differences between the CRE ages of Light and Dark likely reflect recent heating and differences in the relevant diffusion parameters. Based on calculations made with the He diffusion parameters presented by Farley (2002), helium loss due to laboratory preheating of Light seems unlikely for domain sizes larger than 1 μm. By extension, we expect minimal escape of the heavier noble gases. Either ablative or solar heating during transit to Earth can cause losses of ^{3}He$_c$ and ^{4}He (see Schwenzer et al. 2007), and even of ^{21}Ne$_c$ (Heymann et al. 1968). If significant cosmic ray irradiation took place on Mars, then, in principle, impact heating could have led to ^{3}He (and ^{4}He) loss on the Martian surface prior to such loss from a meteoroid in space (Schwenzer et al. 2008).

Our best estimates of CRE ages come from the results for the Dark separate. With production rates modeled after Leya and Masarik (2009) for shielding conditions in bodies with radii between 25 and 100 cm and various depths, we obtain T_{21}(Dark; one-stage irradiation) ~15 Ma. CRE ages based on ^{3}He(Dark) and ^{38}Ar(Dark) range from 7 to 9.5 Ma and agree within the 1σ uncertainties; Busemann et al. (2015) reported a similar CRE age for paired meteorite NWA 8114. Stephenson et al. (2017) and Cartwright et al. (2014) found ^{21}Ne ages older than the corresponding ^{3}He and ^{21}Ne ages in bulk samples (see Table 4). The older ^{21}Ne CRE age of Dark may reflect a higher Na content than reported in Table 2. Cassata et al. (2018) presented CRE ages for five whole-rock samples calculated for various shielding conditions. They observed noncommittally that "reasonable fits to the data are obtained at a depth of 114–116 cm in a meteoroid with a radius of 120 cm, which yields … ^{3}He, ^{21}Ne, and ^{38}Ar exposure ages of 7.7 ± 0.8, 8.9 ± 0.9, and 9.6 ± 1.0 Ma." They also obtained average (n = 4) exposure ages of 12.0 ± 1.7 and 8.7 ± 0.6 Ma based on measurements of cosmogenic ^{78}Kr and ^{83}Kr,

Table 6. Isochron ages (Ma) and intercepts of NWA 7533 and NWA 7034 samples.

		No correction for $^{36}Ar_{Tr}$						Exposure age correction* for $^{36}Ar_{Tr}$					
RUID	K (wt%)	Steps	Age	±	Int	±	MSWD	Steps	Age	±	Int	±	MSWD
NWA 7533													
22219	0.13	AD	1672	37	−124	83	0.82	AD	1562	156	−48	130	0.07
		EH	3006	83	59	310	0.043	EH	2952	20	37	547	0.013
22239	0.27	AD	1487	25	−34	36	6.9	AD	1486	25	−29	43	6.2
22240	0.19	DI	1810	140	970	370	0.38	DI	1880	250	1160	580	0.43
22241	0.41	AJ,#HI	1342	25	203	59	0.74	AJ#CHI	1352	27	215	76	0.47
22242	0.18	AF	758	56	38	44	0.51	AF	806	87	63	54	0.2
22243	0.15	AG	2031	76	−210	110	4.1	AG#H	2100	110	−330	160	1.5
22244	7.95	AG	1356	8	50	55	0.4	All	1358	8	39	68	0.19
NWA 7034													
22220	0.10	CG	1820	470	260	890	0.029	CG	1820	470	260	890	0.029
22221	2.92	EG	1417	19	−34	330	0.33	EG	1417	19	−34	330	0.33
22222	0.17	AF, H	1960	130	−266	87	0.29	AF, H	1960	130	−266	87	0.29
22344	2.78	AP#L	1224	30	1410	100	7.1	AP#L	1224	30	1410	100	7.1
22345	0.18	JQ#P	1840	260	−150	280	0.052	JQ#P	1836	260	−150	280	0.052
22349	1.86	AB, HI	1382	40	620	420	0.09	AB, HI	1382	40	620	420	0.09
22350	1.32	AH	1434	25	85	280	0.097	AH	1434	25	85	278	0.097
22346	0.57	AC, HL, P	1359	50	56	59	0.0.89	AC, HL, P	1506	108	−65	110	0.8
22348	0.27	CDEGHK	1313	5	−100	4.8	5.9	CDEGHK	1313	5	−100	5	5.9

		Minimum $^{36}Ar/^{37}Ar$ correction for $^{36}Ar_{Tr}$						Minimum $^{38}Ar/^{39}Ar$ correction for $^{36}Ar_{Tr}$					
RUID	K (wt%)	Steps	Age	±	Int	±	MSWD	Steps	Age	±	Int	±	MSWD
NWA 7533													
22219	0.13	BD	1663	74	−110	110	0.076	AD	1651	54	−100	93	0.057
		EH	2936	75	58	363	0.033	EH	2950	57	53	312	0.96
22239	0.27	AD	−780	6500	1300	1400	0.53	AD	1504	38	−60	57	4.2
22240	0.19	EG	1972	300	1400	1100	0.0026	DI	1840	290	1010	630	0.11
22241	0.41	AJ#CHI	1850	120	−100	130	0.13	AJ #HI	1369	35	188	63	0.42
22242	0.18	AD, F	3000	10000	−460	4000	0.25	AF	1900	1800	−100	390	0.073
22243	0.15	AD, FG	2072	71	−310	130	0.8	AG	2081	180	−310	170	0.67
22244	7.95	ABCD, FG	1369	19	−51	180	2	BG	1361	7	42	54	0.28
NWA 7034													
22220	0.10	C–G	1850	610	270	1650	0.01	CG	1820	470	260	890	0.029
22221	2.92	EFG	1416	19	−33	330	0.32	EG	1417	19	−34	330	0.33
22222	0.17	A–E, H	1950	190	−260	120	0.2	AF, H	1960	130	−266	87	0.29
22344	2.78	A–P#I, L	1200	68	1370	140	1.3	AP#L	1224	30	1410	100	7.1
22345	0.18	J–O, Q	1900	420	−200	430	0.015	JQ#P	1836	260	−150	280	0.052
22349	1.86	AB, I	1400	NaN	600	NaN	0.0074	AB, HI	1382	40	620	420	0.09
22350	1.32	A–H,#E, G	1130	440	268	460	0.078	AH	1434	25	85	280	0.097
22346	0.57	C, H, I	1270	120	160	360	0.064	AC, HL, P	1493	99	−56	110	0.68
22348	0.27	CDEGHK	1316	8	−110	14	3.0	CDEGHK	1313	5	−100	5	5.9

All fits were carried out with IsoplotR. # denotes excluded. Int = intercept. NaN denotes no meaningful numerical result.
*The exposure age of NWA 7034 and 7533 was taken to be 8.5 Ma (see text). When the total Ca content for a sample calculated from total ^{37}Ar exceeded 10 wt%, an unreasonably high value (e.g., Wittman et al. 2015), the ^{37}Ar signal for every step was reduced by a scaling factor set equal to $10/Ca_{Calc}$. Among the NWA 7533 samples, only 22242 was scaled; all NWA 7034 samples except 22348 were scaled in this way.

respectively. Considering the uncertainties introduced by the differences between the Light and the Dark samples, we believe the results for bulk sample measurements need further investigation and favor a CRE age in the range between 8 and 15 Ma.

$^{40}Ar/^{39}Ar$ Ages

Argon data are presented in Appendix S2 in supporting information. Ages, t, are calculated from the standard relation $t = \frac{1}{\lambda}\ln(J \times R + 1)$ where R is the molar

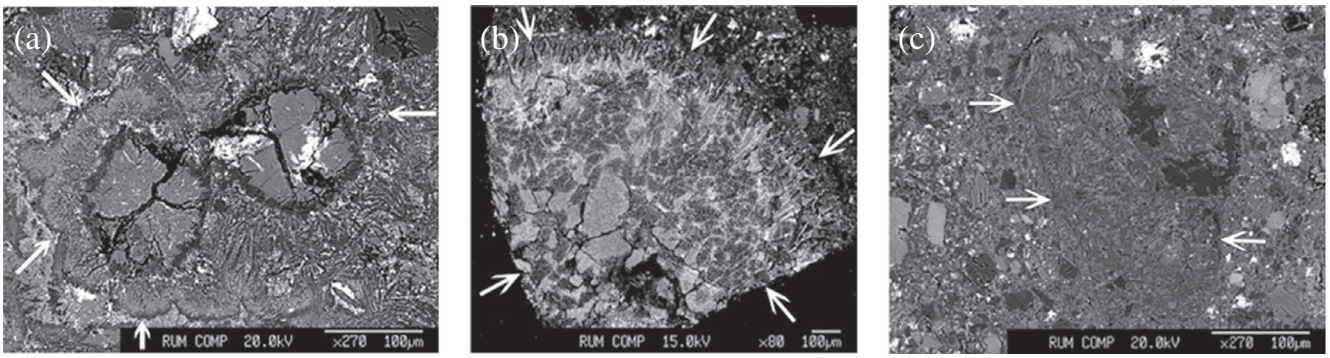

Fig. 2. Backscattered electron images of textures in Chip 7 include quenched fragments (lapilli) thought to be produced by shock-induced melting. White arrows indicate the outer borders of the lapilli. a) A compound object consisting of two central, roughly circular sets of blocky pyroxene grains framed first by cracks (black) that look like spectacles, and then by abutting feldspathic aureoles some 30 μm wide (see also Hewins et al. 2017) (Figs. 4a and 4d). b) A spherule-like lapillus with a lathy border and crystalline clasts at the core. c) Fine-grained clast from a shock melt with irregular inclusions.

ratio of radiogenic ^{40}Ar to K-derived ^{39}Ar (McDougall and Harrison 1988).

While most of the step ages are older than 1.3 Ga, those younger than 1.1 Ga contribute a small but noteworthy percentage, ~5%, to the total. Tables 5 and 6 and Fig. 3 set out the integrated, the plateau, and the isochron ages. Figure 4 places the ^{40}Ar/^{39}Ar ages in the context of other radiometric ages.

Integrated (K/Ar) Ages of Irradiated Samples

The integrated ^{40}Ar/^{39}Ar ages, which are roughly equivalent to K/Ar ages, are given in Table 5 and Fig. 3. They were calculated by summing the measured amounts of ^{40}Ar and ^{39}Ar for all temperature steps. Such ages are useful for a first overview of the results, and for comparisons with the K/Ar ages presented by others, including those from Martian rovers past (Farley et al. 2014) and future. They are unreliable if the sample contained ^{40}Ar when accumulation began (i.e., "trapped" or unsupported argon) or was open to the transport of K and ^{40}Ar thereafter.

Our largest sample, 22348, with a mass of 202 μg (about half the total analyzed), has an integrated age of 1.155 ± 0.003 Ga. The mean of the 16 integrated ages calculated without weighting for sample mass is 1.5 ± 0.4 (1σ) Ga and may serve for comparison with bulk sample measurements. This age agrees with the K/Ar age of 1.56 Ga for NWA 7034 reported by Cartwright et al. (2014), who cautioned, however, that a correction for the presence of nonradiogenic ^{40}Ar would lower the value. Stephenson et al. (2017) found a younger K/Ar age of ~1.3 Ga for the paired stone NWA 7907.

The distribution of integrated ages (Fig. 3) shows that the range for the "plagioclase" samples, from 740 to 2300 Ma, is much larger than the statistical uncertainty of any one age. It also shows that the range of integrated ages of the "plagioclase" (K < 1 wt%) samples is much broader than that of the "alkali feldspars" (K > 1 wt%).

K/Ar Ages for Unirradiated Light and Dark Separates

The measured ^{36}Ar/^{38}Ar ratios of Light and Dark are 5.03 ± 0.08 and 3.73 ± 0.10, indicating the presence of noncosmogenic argon for which ^{36}Ar/^{38}Ar ratio ~0.65. For Light, the measured ^{36}Ar/^{38}Ar ratio is larger than the Martian atmospheric ratio of 4.2 (Atreya et al. 2013). Assuming, therefore, that all the trapped Ar in these separates is terrestrial (^{40}Ar/^{36}Ar = 298.56; Lee et al. 2006) and that cosmogenic ^{40}Ar is negligible, we find radiogenic ^{40}Ar concentrations (10^{-8} cm^3 STP g^{-1}) of 8500 ± 4000 for Light and 3400 ± 1200 for Dark. With K concentrations of 1.8 wt% and 0.76 wt% (Table 2), we obtain K/Ar ages of ~0.9 ± 0.2 Ga for both phases; the uncertainties do not include those of the K concentrations. Corrections for a trapped Martian argon component (^{40}Ar/^{36}Ar = 1900; Mahaffy et al. 2013) yield what we regard as unreasonably young ages: $T_{K/Ar}$(Dark) = 0 and $T_{K/Ar}$(Light) = 0.4 ± 0.1 Ga.

Plateau Ages

Among the 12 samples whose release diagrams satisfy our criteria for the presence of a plateau (Table 5 and Appendix S3 in supporting information), we focus on nine, chosen either because they have good relative precision or because they offer what appears to be reliable new information. For precision, we select six CL-95 plateau ages (CL = confidence limit) and one CL-90 plateau age (Sample, age [Ma]): 22241, 1411 ± 8; 22244, 1361 ± 3; 22221, 1413 ± 8; 22346, 1353 ± 23; 22348, 1284 ± 3; 22350, 1436 ± 9; and 22349 (CL = 0.90), 1416 ± 10. These ages fall within a

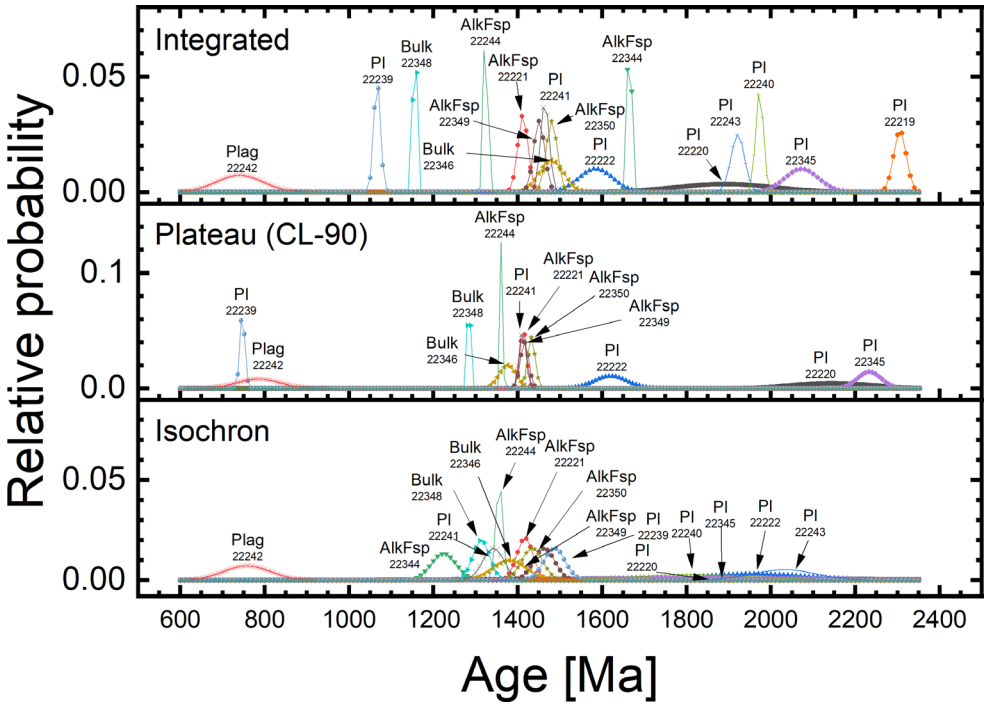

Fig. 3. $^{40}Ar/^{39}Ar$ ages of NWA 7034 and 7533 samples (Tables 5 and 6). (Color figure can be viewed at wileyonlinelibrary.com.)

152 Ma window centered at 1360 Ma. For new information, we call out two plateau ages of lower precision (CL-90) that signal a disturbance within the last ~1.0 Ga, namely 22239, ~747 Ma; and 22242, ~785 Ma. We consider the plateaus of three samples with older apparent ages, 22220, 22222, and 22345, in a later section.

Comparisons with Published Argon-Based Ages

Cassata et al. (2018; their table 1) reported plateau ages for 11 bulk samples of NWA 7034 based on *J*-values obtained with the ^{40}K decay constants proposed by Renne et al. (2011) and an age of 1081 Ma for the standard Hb3gr. From these plateau ages, we calculated an average of 1.33 ± 0.02 (σ_{mean}) Ga. To compare them with ours, we recalculated J-values for our samples in the same way as Cassata and co-workers did for theirs. On average, the recalculations increase the ages measured here by 0.07%, that is, ~1 Ma for a sample with an age of 1.4 Ga. The changes are well within our 1-σ limits of error.

The plateau ages (±1-σ) of 22346 (11 μg; 1.35 ± 0.02 Ga) and 22248 (202 μg; 1.284 ± 0.003 Ga) pertain to small, untreated chips and hence are probably best suited for comparison with, and indeed agree well with the results of Cassata et al (2018) for bulk samples. Excluding the "minibulk" samples 22346 and 22348, the mean plateau ages for the samples of Table 5 are 1.43 ± 0.43 Ga (n = 10; CL-0.90) and 1.50 ± 0.28 Ga (n = 6; CL-0.95). These older ages reflect the broader observation, discussed next, that older step ages are common in the low-K ("plagioclase") samples. Cassata et al. (2018; their fig. 3) report a plateau age of 1374 ± 7 Ma for a feldspathic separate with a K/Ca ratio of ~1. This result agrees well with our results for K-rich grains.

MacArthur et al. (2019; their fig. 17) present release plots for four small samples (<1 mg) from NWA 7034 pair NWA 8114. Three of their release patterns have counterparts in our data: their 2 with our 22220, their 3 with our 22346, and their 4 with our 22243. A fourth sample, 1, has a wide range of ages (<1 Ga to >2.5 Ga) as does our 22350, but unlike it, no plateau. From the results for sample 3, MacArthur et al. inferred that a high-temperature shock event occurred 1.13–1.25 Ga ago.

Minimum Step Ages

Ages generally increase in the release spectra of six low-K samples (Appendix S3). The youngest ages for these samples at low release temperatures place an upper bound on the time of their last disturbance. Table 5 lists these samples, their minimum ages (Ga), and corresponding step identifications: 22219, 1.50 ± 0.07, B; 22240, 1.44 ± 0.01, B; 22243, 1.52 ± 0.02, B; 22220, 1.48 ± 0.06, B; 22222, 1.22 ± 0.04, A; and 22345, 1.45 ± 0.32, I. The minima lie between 1.22 and 1.52 Ga, but most of them are close to or older than the best plateau and isochron

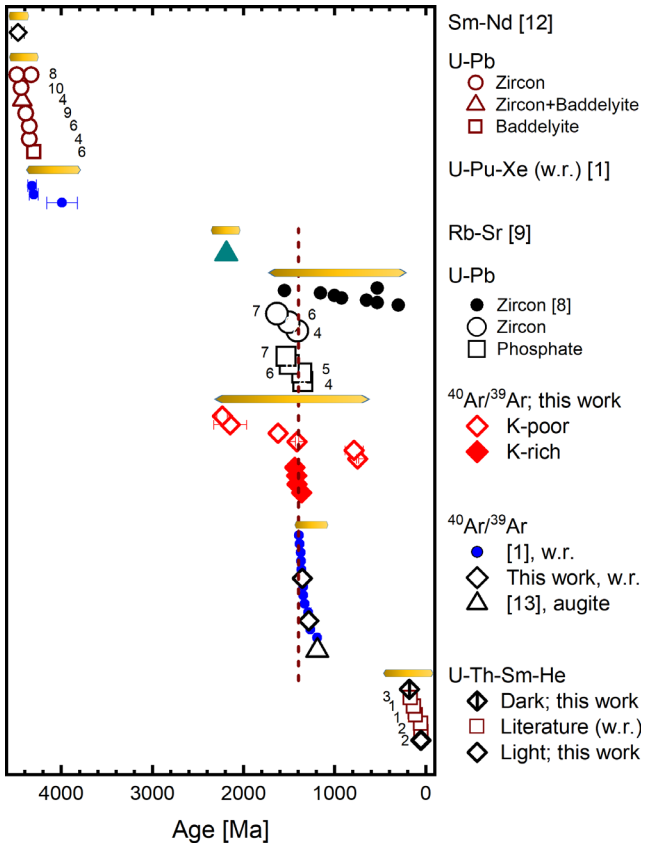

Fig. 4. Radiometric ages of NWA 7034 and pairs after Cassata et al. (2018). $^{40}Ar/^{39}Ar$ ages from this work are the CL-95 plateau ages of Table 5. Graded yellow bars are "umbrellas," covering the ranges for the ages listed beneath. Small digits next to symbols and digits in square brackets denote references given below. w.r. = whole rock. The dashed vertical line is plotted at 1407 Ma, the average of the five most precise plateau ages that include >74% of the ^{39}Ar. [1] Cassata et al. 2018. [2] Stephenson et al. 2017. [3] Cartwright et al. 2014. [4] Yin et al. 2014. [5] Bellucci et al. 2015. [6] McCubbin et al. 2016. [7] Hu et al. 2019. [8] Costa et al. 2020. [9] Agee et al. 2013. [10] Humayun et al. 2013. [11] Bouvier et al. 2018. [12] Nyquist et al. 2016. [13] MacArthur et al. 2019. (Color figure can be viewed at wileyonlinelibrary.com.)

ages, ~1.40 Ga. They are also much older than the minimum of all step ages that we measured, 0.31 ± 0.10 Ga for Step B of 22242. The minimum step age shown in fig. 3 of Cassata et al. (2018), ~0.4 Ga, for their suite of samples is slightly older, but within error limits of our all-sample-minimum value. Barring improbable coincidences, we conclude that while the extent of resetting was highly variable in NWA 7034, many of the K-poor grains bear the stamp of an event or events that took place ~1.40 Ga ago.

Ages also tend to increase in most, but not all, of the release spectrum of 22344, a high-K sample taken from what appeared to be a large single crystal. Uniquely in our sample set, a small fraction of argon released at the lowest heating temperatures (577–749 °C; Appendix S2) gave much older but steadily decreasing apparent ages, from 4.2 Ga to a minimum of 1.7 Ga. At intermediate temperatures, the ages rise from a minimum of 1.3 Ga to a maximum of 1.8 Ga, thus showing incomplete resetting. This sample evidently contained trapped Martian argon.

Older Sample Ages

Taken in comparison to the step ages of the K-rich samples, most of the step ages of the K-poor samples are less precise and span a much broader range, from <1 Ga to >2 Ga, with a bias toward older values (Table A2.1 in supporting information). The lower precision of these step ages reflects poorer statistics associated with smaller ^{39}Ar signals. Their broad range and resistance to resetting point toward uneven conditions 1.4 Ga ago.

Five of our samples have integrated ages older than 1.6 Ga. The most convincing of these "ages" are perhaps those of 22220, for which the integrated (1891 ± 117 Ma), plateau (2145 ± 98 Ma), and highly uncertain isochron (1600–1900 Ma) ages are roughly concordant. Sample 22345 also has consistently old step ages—only step I gives an age younger than 1.5 Ga—but the generally rising release pattern seems more consistent with a single, younger degassing event. Sample 22243 has an integrated age of 1921 ± 16 Ma. A plateau forced through steps C–E (48% of the ^{39}Ar release rather than the 50% required for other plateaus) corresponds to an age 1950 ± 18 Ma. The various isochron ages (Table 6) range from ~2000 to 2100 Ma but are probably inflated by negative intercepts.

Younger Sample Ages

Two low-K samples have distinctly younger ages: 22239 with a three-step plateau (67% of the ^{39}Ar) at 747 ± 6 Ma and 22342 for which five of six step ages are younger than 1.0 Ga. At least one event within the last 0.8 Ga is needed to explain these observations. Nyquist et al. (2016) and provide additional evidence for such an event. Those authors found that Rb/Sr data for "phosphates" and alkali feldspar-enriched samples from NWA 7034 define an apparent age of ~816 Ma.

Isochron Ages

Table 6 and Fig. 5 set out the isochron fitting parameters obtained from IsoPlotR (Vermeesch 2018) for the experimental data treated in four ways (1) without corrections for $^{36}Ar_c$; (2) with such corrections made as described by Cassata and Borg (2016); (3) with such corrections made following the minimum $^{36}Ar/^{37}Ar$

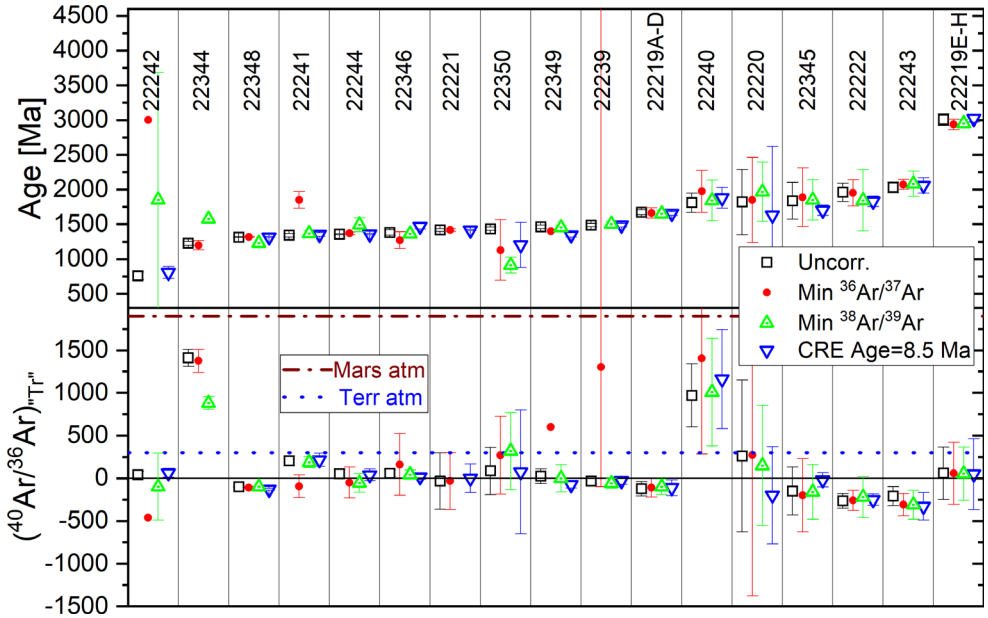

Fig. 5. Isochron fitting parameters obtained in four different ways: 1) without correcting ^{36}Ar for $36Ar_c$; 2) by correcting ^{36}Ar for $36Ar_c$ assuming a cosmic ray exposure age of 8.5 Ma (see Cassata and Borg 2016); 3) by correcting ^{36}Ar for $36Ar_c$ using the minimum $^{36}Ar/^{37}Ar$ method of Garrison et al. (2000); 4) by correcting ^{36}Ar for $36Ar_c$ using the minimum $^{38}Ar/^{39}Ar$ method. (Color figure can be viewed at wileyonlinelibrary.com.)

method of Garrison et al. (2000); and (4) with such corrections made following the analogous, minimum $^{38}Ar/^{39}Ar$ method. To the extent possible, we included the same set of data points in determining the isochrons for each sample. In applying method (2) to 9 of the 16 samples (see Table 6), we scaled the measured ^{37}Ar contents, the precision of which had been degraded by long decay times, to reduce the total calculated Ca content to 10 wt%, a value we regard as the plausible maximum (Wittman et al. 2015). The resulting corrections are thought to be upper bounds. Appendix S3 provides details.

For readability, Fig. 5 shows samples ordered by increasing isochron age calculated without cosmogenic corrections. The corrections for $^{38}Ar_c$ have a modest, favorable effect on the reduced χ^2 statistics (MSWD) of the fits. Without cosmogenic corrections, the average MSWD for 17 isochrons (including both a low- and a high-temperature fit for 22219) is 1.8; application of the three correction lowers this average to values between 0.5 and 1.0. The cosmogenic corrections have only a small effect on the absolute ages and intercepts, however, while generally increasing their uncertainties. We illustrate by comparing the isochron ages of the NWA 7533 samples, for which the ^{37}Ar measurements and hence the cosmogenic corrections are thought to be most reliable. Application of the method of Cassata and Borg (2016) has no systematic effect on the isochron ages of the NWA 7533 samples: Age (T) ratios ($T_{uncorrected}/T_{corrected}$) range from 0.93 to 1.06 and the average value is 1.01 ± 0.04.

Many of the isochrons give nominally negative intercepts. The negative intercepts are not meaningful physically and in most cases are statistically indistinguishable from zero. With only two clear exceptions, 22240 and 22344, the positive intercepts are close to zero. Near-zero intercepts imply the absence from most of the samples of detectable argon derived from the terrestrial or the Martian atmosphere or, more speculatively, from the Martian interior. The small isochron intercepts also suggest that either any trapped ^{36}Ar is planetary, for which the $^{40}Ar/^{36}Ar$ ratio is small, or that any noncosmogenic ^{40}Ar is not associated with ^{36}Ar. Either inference is surprising given that published analyses of bulk samples and our own of Light and Dark show the presence of trapped, mostly terrestrial, ^{36}Ar in NWA 7034. We have no explanation for why Light and Dark but not the irradiated grains should have adsorbed and retained terrestrial argon.

The sample 22344 is exceptional with respect both to the shape of its release pattern (see above) and to the isochron intercepts, which range from 1370 ± 140 to 1510 ± 250, depending on the treatment of trapped ^{36}Ar. We infer that 22344 contains a small amount of Martian atmospheric Ar ($^{40}Ar/^{36}Ar$ = 1900; Mahaffy et al. 2013), in addition to terrestrial atmospheric Ar. The isochron intercepts of sample 22240 also are consistently positive if highly uncertain, ranging from 970 ± 370 to 1160 ± 580. These results imply that ~20% of the total ^{40}Ar in 22240 is trapped and may contain both Martian and terrestrial atmospheric Ar.

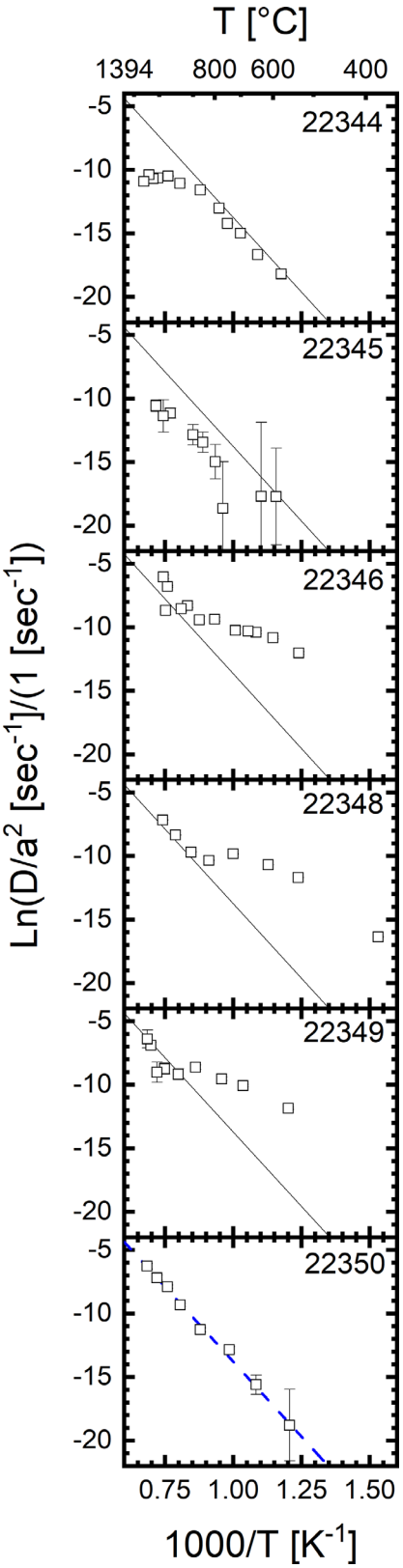

Fig. 6. Arrhenius plots for ^{39}Ar. The dashed line for sample 22350 is a best fit. The solid lines in other plots are copies of that fit. (Color figure can be viewed at wileyonlinelibrary.com.)

We regard the plateau ages as more reliable than the isochron ages for two reasons. (1) The relative uncertainties of the plateau ages are smaller—by a factor of >3 on average; and (2) with only two exceptions (22240 and 22344), the intercepts of the isochrons are analytically indistinguishable from zero. Isochron intercepts of zero imply the absence of detectable trapped argon correlated with ^{36}Ar. While these results do not exclude the possibility that the samples contain unsupported ^{40}Ar, (i.e., ^{40}Ar not correlated with ^{36}Ar), they indicate that isochrons will not help identify it.

Complementarity of Large- and Small-Sample ^{40}Ar/^{39}Ar Analyses

In their fig. 3, Cassata et al. (2018) showed ^{40}Ar/^{39}Ar release patterns for two feldspar separates from NWA 7034 with different average Ca/K ratios. The separate with the lower Ca/K ratios (SUERC-13; Ca/K mostly <2) gave a plateau age of 1374 ± 7 Ma, but no isochron. The sample with the higher Ca/K ratios (LLNL-3; Ca/K mostly >2) gave neither a plateau nor an isochron with step ages ranging from ~1500 Ma to nearly 4000 Ma.

Our results confirm this dichotomy on the microgram scale. The separates SUERC-13 and LLNL-3 studied by Cassata et al. (2018) likely were enriched in material analogous to our high-K and low-K samples, respectively. Four high-potassium grains give plateau ages in a narrow range with an average of 1407 ± 14 Ma, while many low-potassium grains (e.g., 22345) have rising release spectra starting from minimum ages close to 1.4 Ga. Our results also add detail. In four feldspathic separates, Cassata et al. (2018; supporting information) found no apparent step ages that were both younger than 1.0 Ga and modestly precise (relative standard deviation <50%). In contrast, four of our small (mass ≤ 16 μg) samples (22239, 22242, 22349, and 22350) have at least one apparent step age that meets these criteria and two of these samples (22239 and 22242) have several such step ages. The presence of similarly young material throughout NWA 7034 would tend to lower the ages of whole rock samples.

Cassata et al. (2018) measured ^{40}Ar/^{39}Ar ages of 11 whole rock samples of NWA 7034 in a 200 Ma range between 1391 ± 8 (1-σ) Ma and 1191 ± 16 Ma, consistent with our CL-90 plateau ages of 1376 ± 20 Ma and 1284 ± 3 Ma for "minibulk" samples 22346 and 22348, respectively (Table 5). Three of the bulk sample plateau ages reported by Cassata et al. (2018)—those for SUERC-1, 5, and 6—are younger than 1.3 Ga. Cassata et al. (2018) argued that the small uncertainties of these ages require a later,

separate heating event or events. Based on the younger apparent step ages found in some of our samples, we suggest instead that the younger plateau ages for whole rock samples reflect the presence of material that either lost $^{40}Ar^*$ or gained K (possibly as hyalophane) or both, within the last 800 Ma. Of possible interest in this context are the alkali-enriched spherules described by Humayun et al (2019), Sillitoe-Kukas et al. (2019), and Hewins et al. (2017). These spherules are interpreted to be the result of interaction of Ni-rich impact spherules with hydrothermal fluids.

The oldest apparent step age with a modest (<5%) relative uncertainty that we measured was 2946 ± 16 Ma for step E of 22219. Cassata et al. (2018) reported several apparent step ages close to 4 Ga for feldspathic separate LLNL-3. The maximum step ages of three feldspathic clasts (each ~250 μg) analyzed by MacArthur et al. (2019; their fig. 17) ranged from 2600 to 3500 Ma. In view of the generally rising shapes of the release patterns, we believe that all these old ages are consistent with partial degassing of ancient feldspathic minerals that became part of the breccia.

One inconsistency between the results for low-mass and for high-mass samples concerns the intercepts of standard isochrons ($^{40}Ar^*/^{36}Ar$ versus $^{39}Ar/^{36}Ar$). With outliers 22240 and 22344 (Fig. 5) excluded, the mean intercepts (±1-σ mean) for the four sets of calculations summarized in Fig. 5 for our low-mass samples are indistinguishable from zero: 30 ± 53 (no cosmogenic corrections), 163 ± 132 (minimum $^{36}Ar/^{37}Ar$ method), 34 ± 74 (minimum $^{38}Ar/^{39}Ar$ method), and −54 ± 35 (CRE age correction), respectively. In contrast, Cassata et al. (2018; their fig. 2) determined a mean intercept of 576 ± 104 for seven whole rock samples; the isochrons for these samples include only data for lower temperature steps in order to focus on the contributions from felsic phases. A relaxed view of the 2-σ error limits reconciles the two means, but this is not the first time that we have obtained near-zero intercepts for small Martian samples (Lindsay et al. 2012). In whole rock samples, the release of argon from various components with different ages but no trapped Ar might lead to a clockwise rotation of the "isochron" for a bulk sample, particularly if high ages predominate at higher temperatures and lower $^{39}Ar/^{36}Ar$ ratios.

^{39}Ar Diffusion Parameters

Figure 6 shows Arrhenius plots constructed from ^{39}Ar data obtained as described by Setera et al. (2020) for six samples of NWA 7034 (for details, see Appendix S4 in supporting information). Numerical values of the fitting parameters are given in Table 7; Arrhenius plots and data for all Ar isotopes are presented in Appendix S4. The results for 22350 are the simplest. For ^{39}Ar, the plot is linear over the entire range. The best-fit slope corresponds to an activation energy of 193 ± 10 kJ mol^{-1}, a value toward the low end of the range for terrestrial K-rich feldspars (175–286 kJ mol^{-1}; Cassata and Renne 2013; their table 2). Assuming an average grain mass of 1 μg and a density of 2.7 g cm^{-3} yields a "radius" of ~43 μm for the average "domain size," a, of our sample 22350. Substitution of a = 43 μm into the intercept of the best fit, $D_0/a^2 = 1.3 \times 10^4$ s^{-1}, gives $D_0 \sim 2.5 \times 10^{-5}$ m^2 s^{-1}, midrange between the extrema of 4×10^{-8} m^2 s^{-1} and 2 m^2 s^{-1} reported by Cassata and Renne (2013; their table 2).

To make it easy to compare the results for different samples, we have reproduced the best fit to the ^{39}Ar data from 22350 on all the Arrhenius plots of Fig. 6. If the release patterns were dominated by a single, widely distributed, and well-defined phase, then we would expect similar activation energies ($E_a = -1 \times \text{slope} \times R$, where R is the gas constant) for ^{39}Ar in all samples. Many of the results, though not all of them, are consistent with this expectation. The low temperature data points for sample 22344, for example, give $E_a(^{39}Ar)$ = 192 ± 9 kJ mol^{-1}, while at higher temperatures, the data points are displaced downward from the fit, probably because of the onset of melting (e.g., Cassata and Renne 2013; their fig. 1). The activation energy of 173 ± 48 kJ mol^{-1} for ^{39}Ar in 22345, a K-poor sample, just agrees within the 1-σ uncertainties with the activation energy of 22350, while the values of D_0/a^2 are generally lower.

Three samples show more complex behavior, but at higher temperatures, selected (perhaps with bias) data give values of E_a close to that of 22350: 22346, 213 ± 21 (steps GHIKL); 22348, 203 ± 22 kJ mol^{-1} (steps FGH); and 22349, 208 ± 42 kJ mol^{-1} (steps E–I). We conclude that for the most part, at high temperatures, the diffusion of ^{39}Ar behaves as expected for feldspathic material.

Lower Apparent Activation Energies for ^{39}Ar in 22346, 22348, and 22349

The Arrhenius plots for ^{39}Ar from 22346 ("bulk"), 22348 ("bulk"), and 22349 ("alk fsp") are flatter at lower temperatures, T, than at higher ones, with a rough division point at T [K] ~ 1100 ± 100. Fits to the low-T regions yield low activation energies of ~80 to 100 kJ mol^{-1}, less than half the value characteristic of many feldspathic minerals. The change in slope suggests the presence of more than one phase, which seems unsurprising in the minibulk samples 22346 and 22348 but was unexpected for 22349.

Table 7. Activation energies (E_a), diffusion parameters (D_0/a^2), closure temperatures (T_c), and cooling rates at T_c $\left((dT/dt)|_{T_c}\right)$ of NWA 7034 samples.

Sample (steps)	Age Ma	E_a kJ mol^{-1}	Ln(D_0/a^2)[d]	T_c °C	$(dT/dt)\|_{Tc}$ K Ma^{-1}
Conventional cooling rate calculation[e]					
22344[a] (A–F)	–	192 ± 9	8.6 ± 1.1	254 ± 27	−10
22345[b] (F–K)	–	173 ± 48	4.8 ± 4.2	245 ± 150	−10
22346[c] (A–D)	–	82 ± 10	0.3 ± 1.4	8 ± 35	−10
22348[c] (E–H)	–	168 ± 11	7.7 ± 1.1	198 ± 32	−10
22349[a] (A–D)	–	79 ± 5	−0.3 ± 0.7	2 ± 18	−10
22350[a] (A–G)	–	193 ± 10	9.5 ± 1.0	246 ± 29	−10
Coupled cooling rate calculation[f]					
22350	1436 ± 9	193 ± 10	9.5 ± 1.0	239	−5.6
22346[g]	1353 ± 23	82 ± 10	0.3 ± 1.4	−5	−1.5
22350	1436 ± 9	193 ± 10	9.5 ± 1.0	256	−25
22349	1416 ± 10	79 ± 5	−0.3 ± 0.7	0	−6.6

[a]K-rich.
[b]K-poor.
[c]Bulk.
[d]The natural logarithm requires a dimensionless argument, here the magnitude of D_0/a^2 stripped of its units of s^{-1}.
[e]Closure temperature calculated from Equation S6.1 (see Dodson 1973) assuming a cooling rate at closure of −10 K Ma^{-1}. Uncertainties calculated as in Setera et al. (2020).
[f]See text and Appendix S6 in supporting information.
[g]Use of the diffusion parameters for steps A–H (Appendix S4) gives an unreasonably low closure temperature for 22346 of −44 °C.

We considered several possible sources of the Ar released with lower activation energy at low temperature. Most terrestrial feldspars have higher activation energies (see Cassata and Renne 2013). Cassata and Renne (2013; their fig. 17) observed Arrhenius plots for Na-rich feldspar with distinct, parallel, low- and high-temperature segments, offset by a kink. Both segments, however, have the same high activation energies, which is not the case for our Arrhenius plots.

One K-rich member of the feldspar group of potential interest is hyalophane. In NWA 7034 and paired stones, Hewins et al. (2017) identified hyalophane (Ba-, K-feldspar) within secondary veins crosscutting large vitrophyric clasts. Sillitoe-Kukas et al. (2019) and Humayun et al. (2019) identified several devitrified impact melt spherules that contained hyalophane in veins and high levels of K and other alkali elements in the vitrophyric matrix. In terrestrial environments, hyalophane is "dominantly a hydrothermal mineral" (Hewins et al. 2017) and indicates very low grade (anchizonal to epizonal) conditions and alteration by Ba-bearing fluids in the ~160° to 350° temperature range (Tasáryová et al. 2014). Palinkaš et al. (1996; their fig. 2) reported an Ar activation energy of 147 ± 16 kJ mol^{-1} for a terrestrial hyalophane. While it seems unlikely that hyalophane was present in large enough amounts to have had a major effect on the argon budget of larger samples, it may have influenced those of smaller ones.

Phyllosilicates generally have higher activation energies (Harrison et al. 1985, 2009; Vardzelashvili et al. 1988), and are uncommon in NWA 7034, less than a few % according to Muttik et al. (2014). Harrison and McDougall (1982) reported lower activation energies, ~120 kJ mol^{-1} for microcline, which to our knowledge does not occur in NWA 7034.

Studies of bulk meteorites have yielded a range of argon activation energies. Typically, but not always, such studies give higher values, >150 kJ mol^{-1} (Fechtig et al. 1963; Turner et al. 1978). The H-chondrites Sena (H4; E_a = 92 kJ mol^{-1}) and Tieschitz (H3; E_a = 100 kJ mol^{-1}) furnish counter examples, having activation energies comparable to those of 22346, 22348, and 22349. Fechtig et al. (1963; their fig. 2) showed that ^{37}Ar produced by neutron irradiation in stony meteorites of several types was released in two portions during stepwise heating (1) a low-T portion with low E_a and (2) a high-T portion with high E_a. They associated the lower activation energy with diffusion along structural defects.

Enhanced diffusivities of K are known for materials shocked and annealed in the laboratory (Ostertag and Stöffler 1982); low argon activation energies are known for natural samples (Weirich et al. 2012; e.g., CA2 of their fig. 9 and their table 6) and for certain lunar glasses (Gombosi et al. 2015; their fig. 6), especially those with lower degrees of polymerization (higher fractions of nonbridging oxygen

atoms). Although maskelynite has not been reported in NWA 7034 (Agee et al. 2013; Cartwright et al. 2014), Wittmann et al. (2014) note that "Most vitrophyric melts, spherules, and fine-grained crystallized clasts with xenoliths are likely impact products, recording shock pressures >80 GPa," citing Stöffler and Grieve (2007) as the authority. Weirich et al. (2012) concluded that "The formation of glass or maskelynite is apparently not required to lower the activation energy of feldspar." It seems plausible, then, that the structures of the Arrhenius plots for 22346, 22348, and perhaps 22349 owe to the presence of glass or perhaps to the less dramatic effects of shock disordering in feldspathic phases that have been shocked and annealed. MacArthur et al. (2019) observed a glassy, K-rich phase in NWA 8114, an NWA 7034 pair. Those authors interpreted the phase as a product of pyroxene oxidation at high temperatures reached in the aftermath of an impact.

Diffusion Parameters From $^{36,37,38,40}Ar$

The diffusion parameters obtained from $^{36,37,38,40}Ar$ (Appendix S4) do not provide much additional information. For samples with flat release patterns, ^{40}Ar and ^{39}Ar should and do give essentially the same results. To the degree that Ca and K reside in the same phases, reactor-produced ^{37}Ar and ^{39}Ar should diffuse in similar ways and visual examination of Fig. A4.1 in supporting information suggests broad consistency. The two isotopes, however, are well correlated ($R > 0.8$) in only one sample, 22350, perhaps because of the poor precision of the ^{37}Ar measurements. Samples 22344, 22346, and 22348 have very low $^{36}Ar/^{38}Ar$ ratios due, we think, to neutron activation of Cl in apatite, which took place during sample irradiation. We searched for but found no trends in the ^{38}Ar diffusion parameters associated with higher Cl contents.

U-Th-Sm-^{4}He Ages

The U/Pb ages of the chlorapatite in NWA 7034 were reset ~1.4 Ga ago (Bellucci et al. 2015). If lead isotopes were reset, it seems safe to infer the loss of all radiogenic ^4He accumulated prior to that time. By assuming the bulk U, Th, and Sm contents of 0.51, 2.64, and 6.43 ppm of Agee et al. (2013), respectively (see Table 2), we estimate that a maximum radiogenic ^4He concentration of $21{,}000 \times 10^{-8}$ cm^3 STP g^{-1} could have accumulated in the last 1.4 Ga.

The measured ^4He concentrations (10^{-8} cm^3 STP g^{-1}) for bulk samples are in fact about an order of magnitude lower: 2420 (Cartwright et al. 2014); 2300 and 2700 (Stephenson et al. 2017); 1629 and 1717 (Cassata et al. 2018). Our measured values for ^4He (not corrected for a small amount of cosmogenic ^4He) in unirradiated separates Dark (4100) and Light (120) bracket the results for the bulk samples. To estimate the ^4He content of a bulk sample from the results for Light and Dark, we write by analogy to Equation S1.1 (Appendix S1)

$$\begin{aligned} {}^4He_{bulk} &= {}^4He_{Dark}\left(1 - \left[f_{alk\ fsp} + f_{plag\ fsp}\right]\right) \\ &\quad + {}^4He_{Light}\left(f_{alk\ fsp} + f_{plag\ fsp}\right) = 2700 \pm 270 \end{aligned} \quad (1)$$

and obtain the result $^4He_{bulk} = 2700 \pm 270 \times 10^{-8}$ cm^3 STP g^{-1}, which is similar to the values reported for bulk samples.

Phosphates, principally apatite, are presumably the major host for the isotopes of U, Th, and Sm that produced the radiogenic ^4He in the Light separate. The EDX spectra indicate that Light contains ~0.28 wt% P (Table 2), which implies the presence of ~1.58 wt% of apatite in Light (based on P_2O_5 0.41 wt% in apatite; McCubbin et al. 2016; their table S6). To estimate the U-Th-Sm/^{4}He age of Light, we take for apatite U = 4.37 ppm, Th = 30.7 ppm (McCubbin et al. 2016; table S7) and Sm = 94 ppm (from Sm/U = 21.5 [mass/mass; Min et al. 2017; their table 1]). Multiplying these concentrations by the quantity 0.0158 g apatite/(g Light) yields U = 0.07 ppm, Th = 0.48 ppm, and Sm = 1.48 ppm in Light and a U-Th-^{4}He age of 54 Ma.

In the primarily pyroxenitic Dark separate, the U and Th budgets are dominated not by apatite, but by zirconium-bearing minerals (Cassata, personal communication; Humayun et al. 2019). As we do not know the Zr content of Dark, to estimate U and Th contents, we rely on a mass balance calculation analogous to the one done for ^4He by using Equation 1. With U = 0.51 ppm, Th = 2.64 ppm in bulk NWA 7034 (Agee et al. 2013; their table S2), $f_{alk\ fsp} + f_{plag\ fsp} = 0.429$, and the U and Th contents for Light given above, we obtain for Dark U = 0.85 ppm and Th = 4.25 ppm. In Dark, samarium is hosted primarily by apatite and so we follow the method of calculation adopted above for Light. Specifically, for Dark, the measured phosphorus content of 0.42 wt% (Table 2) corresponds to 2.36 wt% apatite, and hence to an Sm content of 2.2 ppm. With these results, we calculate a U-Th-^{4}He age of 181 Ma. Stephenson et al. (2017) and Cartwright et al. (2014) reported similar U-Th-^{4}He ages of ~180 Ma for bulk NWA 7034 or paired samples. Cassata et al. (2018) obtained for whole rock fragments of NWA 7034 somewhat lower values of 135 ± 6 and 113 ± 4 Ma, which lie between our values for Light and Dark.

The large age difference between Dark and Light implies the recent loss of ^4He from chlorapatite and probably from feldspathic minerals as well. The

evidence for loss of (cosmogenic) ^{3}He from Light (Appendix S1) strengthens this inference. As ^{3}He and ^{4}He have nearly equal diffusion parameters (Cherniak et al. 2009; Farley 2018), it is reassuring that the ratios $^{3}He_c$(Light)/$^{3}He_c$(Dark) = 0.06 ± 0.05 and ^{4}He (Light)/^{4}He(Dark) = 0.03 ± 0.01 are similar in magnitude.

DISCUSSION

Summary of Ar/Ar Age Results

The five most convincing plateau ages—those with 1σ uncertainties of 20 Ma or less and based on at least 75% of the ^{39}Ar released—lie in a narrow window between 1.36 and 1.42 Ga (Table 5; Fig. 4). Four of these ages pertain to K-rich grains: 22221, 1413 ± 8 Ma; 22244, 1361 ± 3 Ma; 22349, 1416 ± 10 Ma; and 22350, 1436 ± 9 Ma; and have an average of 1407 ± 16 Ma (1-σ mean). The fifth pertains to a K-poor grain: 22241, 1411 ± 8 Ma. Inspection of the release plot of 22350 and, arguably, that of 22349, reveals a few older step ages at higher temperatures. The fractions of ^{39}Ar released in these steps, however, are small and/or the age uncertainties large. We believe that these older ages indicate the presence in the sample of some older, low-K material (plagioclase). Sample 22244 appears to be an outlier: Its age differs from the average of the other four by nearly 3σ. A Grubbs test, which takes no account of the individual uncertainties, for all five ages returns the result that 22244 is "furthest from the rest, but not a significant outlier ($P > 0.05$)." The mean for the five is 1407 ± 13 Ma (1-σ mean); we adopt this value as the best estimate for the time of a major thermal event that reset the argon clocks in NWA 7034. In general, the ages measured for K-poor grains are more dispersed, from 0.3 to 2.9 Ga, and give proportionally fewer plateaus than do the K-rich grains.

Comparison of ^{40}Ar/^{39}Ar ages with U-Pb Ages

The U-Pb ages summarized in Table 1 and Fig. 4 indicate crystallization ~4.5 Ga ago and a major disturbance within the last 1.6 Ga. The younger, disturbed ages (Ma) range from 1410 ± 56 to 1634 ± 93 for zircons and from 1345 ± 47 to 1530 ± 65 for phosphates (Humayun et al. 2013; Yin et al. 2014; Bellucci et al. 2015; Hu et al. 2019). Zircon ages appear to be older, on average by ~93 ± 132 Ma (1-σ), but the uncertainty of the difference is large. Our best estimate of 1407 ± 13 Ma for the time of a major resetting of ^{40}Ar/^{39}Ar ages fits comfortably within the range of phosphate ages; less agreeably, it occupies the younger edge of the zircon age distribution. We are inclined to chalk off the latter observation to the uncertainties of the zircon ages for three reasons. (1) We see ample evidence for partial resetting of the ^{40}Ar/^{39}Ar ages at 1.40 Ga and no evidence considered fully persuasive for well-defined ^{40}Ar/^{39}Ar ages older than 1.40 Ga. (2) As discussed in the next two sections, it is difficult to reconcile the observed distribution of ^{40}Ar/^{39}Ar ages with a thermal history in which NWA 7034 took up to 100 Ma to cool from the lead to the argon closure temperature. (3) Yin et al. (2014) reported no significant differences between the U-Pb ages of apatites and zircons. Hu et al. (2019) comment that "The metamorphic event recorded in apatites should be close to or the same as the resetting event happened in metamict zircons."

Heating and Alteration ~1.4 Ga Ago

A disturbance or disturbances in most parts of NWA 7034 ~1.4 Ga ago reset the argon and some of the lead clocks (Tables 1 and 5) in NWA 7034. We use the thermal diffusion parameters measured for the NWA 7034 samples to estimate the total duration heating that could account for the observations, and conclude that it probably did not last more than 100 yr. In effect, the diffusion parameters are a way to smooth the gas losses observed in the laboratory after 120 s of heating at various temperatures and to extrapolate them to the losses expected after much longer heating times at those same temperatures. We believe that despite their uncertainties, the diffusion parameters are sturdy enough to carry the weight of these calculations (see Setera et al. 2020).

With the higher activation energies (~200 kJ mol^{-1}) of ^{39}Ar measured for high-temperature releases, we can estimate the isothermal heating time required to expel a given fraction of the radiogenic ^{40}Ar formed in the 3 Ga period between 4.4 and 1.4 Ga. Such calculations are of interest primarily for the K-poor samples exemplified by 22345 and 22240, whose ages rise from 1.4 Ga with increasing release temperature. Obversely, the lower activation energies of ^{39}Ar measured in the minibulk samples 22346 and 22348 and in 22349 can be used to estimate maximum heating times allowed before losses occurring within the last 1.4 Ga—losses that are *not* indicated by the data—would have become noticeable.

Approximate Equations 2a and 2b relate a given fractional loss, F_{lost}, of ^{40}Ar* to the heating time t:

$$t = \frac{1}{3}\left[\left(\frac{6}{\pi} - F_{lost}\right) - \frac{6}{\pi}\sqrt{1 - \frac{\pi}{3}F_{lost}}\right]\left(\frac{D_0}{a^2}\right)^{-1} e^{+\frac{E_a}{RT}};\ F_{lost} \leq 0.9 \quad ((2a))$$

or

$$t = -\frac{1}{\pi^2}\ln\left[\frac{\pi^2}{6}(1-F_{\text{lost}})\right]\left(\frac{D_0}{a^2}\right)^{-1} e^{+\frac{E_a}{RT}}; 0.9 < F_{\text{lost}} < 1.0 \quad ((2b))$$

Use of these equations assumes that the total time over which heating occurred was short compared to the half-life of ^{40}K (1.25 Ga). Appendix S5 in supporting information explains the calculation of F_{lost} and further details. In applying Equation 2, we assume that the seven samples with rising release patterns and low-temperature, apparent step ages close to 1.4 Ga (1) formed 4.4 Ga ago (Nyquist et al. 2016), and (2) were partially degassed ~1.4 Ga ago, but not since then. Table 8 lists the seven samples that meet the two stated criteria and the ^{40}Ar loss inferred for each one. With an assumed activation energy of ~190 kJ mol^{-1}, the losses at 1.4 Ga range from 85% for 22219, a K-poor sample, to 96% for 22344, the one K-rich sample among the seven. The heating times required to cause these losses are short, from 10 to 50 yr at 500 °C and from a few minutes to a few hours at 1000 °C (see also Fig. 7a). The additional time needed to boil off all but 1% of the remaining $^{40}Ar^*$ is of the same order of magnitude.

As noted above, several K-rich grains evidently retain little or no ^{40}Ar generated prior to 1.4 Ga. It is, therefore, important to understand the conditions that allow both the preservation of "ancient" ^{40}Ar in K-poor grains and the removal of "ancient" ^{40}Ar from K-rich grains. The diffusion parameters determined for the one K-poor sample (22345) and one K-rich sample (22350) in Table 7 are generally consistent with the option of greater removal of ^{40}Ar from K-rich material: Their magnitudes are such that at 500 °C, it would have taken, for example, about twice as long, 22 yr, for K-poor 22345 to lose 90% of its ^{40}Ar 1.4 Ga ago as for 22350 (K-rich) to lose 99% of its ^{40}Ar, ~10 yr. At 1000 °C, the times are 0.7 and 5 h, respectively. The uncertainties of this calculation are large, however, and it is not obvious that the difference between the diffusion parameters of these two grains carries over to other samples.

We have been assuming that the 1.4 Ga ages of the K-rich grains reflect ^{40}Ar losses due to thermal diffusion. A complementary alternative is to reset the argon clocks through lower temperature processes associated with hydrothermal activity 1.4 Ga ago and prior shock. Specifically, either one impact event at ~1.4 Ga or several earlier ones might have shocked some of the feldspar enough to induce a state of disorder that made it susceptible to annealing and reorganization of the crystal lattice in the presence of a hot and briny fluid phase. Extensive exchange of K between a brine and the shocked feldspar can occur on timescales of hours to days (Ostertag and Stöffler 1982) permitting full or partial resetting of the $^{40}Ar/^{39}Ar$ clock for the individual felsic grains in the breccia. We explore this possibility further in the section on a possible relationship between NWA 7034 and the nakhlites and chassignites.

Table 8. Fractional radiogenic ^{40}Ar losses for samples with rising temperature release patterns and isothermal heating times required to achieve those losses.

RUID	F_{lost}	t (F_{lost}) (yr at 500 °C)	t_{99}	Δt_{99}	$t(F_{\text{lost}})$ (h at 1000 °C)	t_{99}	Δt_{99}	Diff Par
22219	0.85	3.6	10.6	7.0	0.2	0.7	0.5	22350
22240	0.91	5.1	10.6	5.6	0.3	0.7	0.4	22350
22243	0.92	5.2	10.6	5.4	0.3	0.7	0.4	22350
22220	0.93	5.4	10.6	5.2	0.4	0.7	0.3	22350
22222	0.95	6.5	10.6	4.1	0.4	0.7	0.3	22350
22345	0.90	22.5	50.4	27.9	4.9	11.1	6.1	22345
22344	0.96	13.4	20.9	7.5	1.0	1.5	0.5	22344

F_{lost} = Fraction of radiogenic ^{40}Ar lost 1.4 Ga ago as calculated in Appendix S5; $t(F_{\text{lost}})$ = Time required at the indicated temperature to lose the fraction F_{lost} of the radiogenic ^{40}Ar accumulated period between 4.4 Ga and 1.4 Ga B. P.; t_{99} = As for $t(F_{\text{lost}})$ but for a loss of 99% of the radiogenic ^{40}Ar accumulated period between 4.4 Ga and 1.4 Ga B. P.; $\Delta t_{99} = t_{99} - t(F_{\text{lost}})$.
The column Diff Par identifies the sample from which the diffusion parameters, which are listed in Table 7, were taken.

Post 1.4 Ga Disturbances and a Terrestrial Age for NWA 7034

Several authors have discussed the plentiful evidence for thermal disturbance of NWA 7034 within the last 1.4 Ga. Cassata et al. (2018) reported young (<1.3 Ga) apparent ages for lower temperature steps of samples LLNL-2, SUERC-2, and SUERC-5. McCubbin et al. (2016, their fig. 11) pointed out indications of a disturbance within the last 1.4 Ga of the U-Pb ages of "young" zircons. Costa et al. (2020) reported six concordant zircon ages between 0.2 and 1.2 Ga. To this partial list, we add the younger apparent $^{40}Ar/^{39}Ar$ step ages of 22239, ~700 Ma; 22242, ~700 Ma; and 22348, 700–1000 Ma. We now examine the maximum extent of heating compatible with the amounts of argon that the samples retained.

Figure 7b shows the maximum duration of heating at various temperatures, which if carried out today would preserve the radiogenic ^{40}Ar accumulated over the last 1.4 Ga as observed in several of our samples. Significant heating of the intact meteorite for longer times during that interval would have lowered significantly, that is, by >0.2 Ga, the minimum apparent step ages of most of our K-poor samples and the 1.4 Ga plateau ages of the K-rich samples, contrary to observation. For example, only one day of heating of

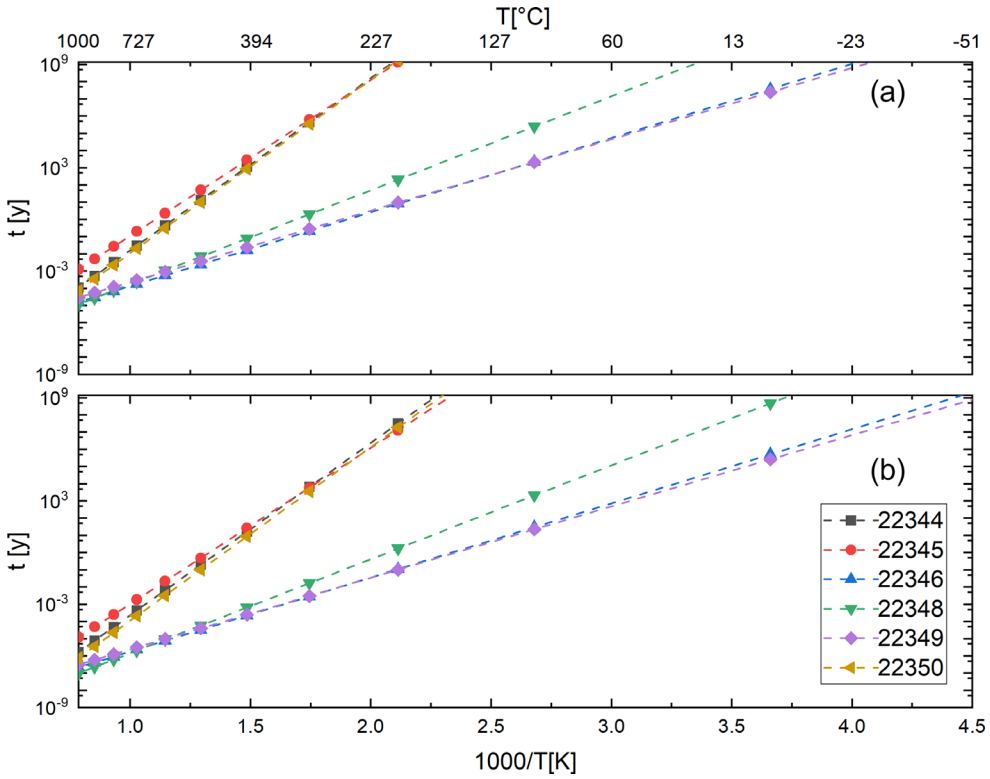

Fig. 7. The times required at various temperatures for the samples listed to lose quickly (a) the $^{40}Ar^*$ accumulated between crystallization 4.4 Ga ago and a major thermal event ~ 1.4 Ga ago and (b) 20% (an upper bound permitted by the data for selected samples) of the $^{40}Ar^*$ accumulated between a major degassing event ~1.4 Ga ago and the present. Calculational details are in Appendix S5. (Color figure can be viewed at wileyonlinelibrary.com.)

sample 22349 is allowed at 300 °C ($1000/T = 1.75$ K^{-1}), and about 10 s at 1000 °C.

The problem of argon retention in 1.4 Ga old samples is heightened by the "young" (~750 Ma) ages of 22239 and 22242. If due to heating alone, these young ages would imply ^{40}Ar losses of ~50%. One possible explanation is that 22239 and 22242 were heated as separate objects and incorporated late in the history of the meteorite, as suggested by Cassata et al. (2018) and Costa et al. (2020). Alternatively, rather than loss of ^{40}Ar at higher temperatures, these two samples may have experienced hydrothermal alteration at lower temperatures with the addition of potassium. Potassium addition is consistent with the observation of secondary veins of hyalophane crosscutting large vitrophyric clasts and impact melt spherules (Hewins et al. 2017; Humayun et al. 2019; Sillitoe-Kukas et al. 2019).

We also entertained the possibility that the young ages of 22239 and 22242 reflect ^{40}Ar loss due to ablative heating. This hypothesis comports with the observation of a fusion crust on and the small recovered mass, 84 g, of NWA 7533 (the source of 22239 and 22242). A mass of 84 g corresponds to a pre-atmospheric "radius" of only a few cm and in such a small body, all matter would have lain within warming distance of the surface. To account for the full range of $^{40}Ar/^{39}Ar$ ages in NWA 7533 samples, however, we must appeal ad hoc to highly selective heating of 22239 and 22242, which seems improbable.

At Martian surface temperatures of up to ~−60 °C (see Wordsworth 2016), even the samples with ^{40}Ar activation energies of ~100 kJ mol^{-1} retain 80% or more of the ^{40}Ar produced for 1.4 Ga (Fig. 7b). Humayun et al. (2016) showed that NWA 7034 spent most of its time on Mars at depths greater than 2–3 m. With geothermal gradients as low as 6–10 K km^{-1} (Hoffman 2001), heating at the temperatures found at depths up to ~1 km would have had little effect on the ^{40}Ar inventory.

To estimate a terrestrial age for NWA 7034, we consider sample 22349, which has a CL-90 plateau age of 1416 ± 10 Ma (Table 5) and a low activation energy of 79 ± 5 kJ mol^{-1} (Table 7). If we assume a constant, mean Moroccan temperature of $T = 25$ °C ($1000/T = 3.35$ K^{-1}) and that 22349 lost no more than 20% of its radiogenic ^{40}Ar, then from Fig. 7b, we read a maximum terrestrial age of ~14 ka. Diurnal excursions to higher temperature would lower this estimate; an underestimated value of D_0/a^2 would raise it. A terrestrial age of 14 ka is in line with those of other hot

desert meteorites (Jull 2006). It is of interest to consider helium retention in this context. Assuming the diffusion parameters for He in apatite (E_a = 138 kJ mol^{-1}; D_0 = 0.005 m^2 s^{-1}; fig. 3 of Farley 2002) and a domain size of 1 μm, we estimate that at T = 25 °C, NWA 7034 would retain ~80% of its He after 14 ka.

For completeness, we consider losses of Ar that might have occurred during sample irradiation. Our samples were irradiated at the TRIGA reactor in Denver for which Dalrymple et al. (1981) have reported temperature measurements. Those authors determined an upper limit of T_{irrad} = 90 °C for the water-cooled "central thimble," the location of sample irradiation, and a value of 70 °C for the "rabbit tube," a nearby location in the outer ring of the reactor (see their fig. 2). From these results, Dalrymple and co-workers infer that the temperature in the central thimble was between 70 and 90 °C. With the diffusion parameters measured for our samples, we can estimate the fractional losses of argon expected after an 80 h irradiation at various temperatures, T_{irrad}. Such losses are negligible at 90 °C for all our samples. Even with T_{irrad} = 200 °C, our least retentive sample, 22349 (E_a = 79 kJ mol^{-1}), loses only 7% of its ^{39}Ar. A loss of this size would not affect our conclusions.

Closure Temperatures and Cooling Rates at Closure

Closure temperatures, T_c, are widely used in constructing thermal histories of extraterrestrial materials (e.g., Kleine et al. 2008). Here, we calculate closure temperatures for $^{40}Ar/^{39}Ar$ in NWA 7034 and 7533 samples with two slightly different methods, both based on the work of Dodson (1973). Method 1 is conventional: We calculate T_c from argon diffusion parameters by assuming a numerical value for the cooling rate at T_c, $(dT/dt)|_{T_c} = -10$ K Ma^{-1}, and solving iteratively Equation S6.1 of Appendix S6. Results are presented in Table 7; the closure temperatures are high enough to allow preservation of ^{40}Ar under ambient surface conditions on Mars (T < 0 °C).

Method 2 is based on the observation that by identifying two samples that share a common thermal history but have different, known activation energies and ages, we can eliminate the need to assume a cooling rate. We summarize here the results of applying this approach to two pairs of samples: 22350/22346 and 22350/22349 but defer to the next section a discussion of the extended temperature history. Appendix S6 presents the mathematical details of the method and the rationale for and the shortcomings of these sample choices.

The cooling rates calculated for 22350 at closure, T_c = 243 °C and 256 °C, are ~−6 and ~−25 K Ma^{-1} for the 22350/22346 and 22350/22349 combinations, respectively (Table 7). The results are similar to those obtained by assuming $(dT/dt)|_{T_c} = -10$ K Ma^{-1}. Cassata and Renne (2013, their fig. 23 and their table 4) reported results comparable to those for 22350 in terrestrial feldspars cooling at an assumed rate of −10 K Ma^{-1}. The closure temperatures (~−5 °C and 0 °C) and the cooling rates at closure, T_c (−1.5 K Ma^{-1} and −6.6 K Ma^{-1}) for 22346 and 22349 are lower and slower, respectively. The differences in the cooling rates at comparable closure temperatures reflect the factor-of-four difference in the spread of the ages of the samples selected, t_{22350}–t_{22346} =83 Ma versus t_{22350}–t_{22349} = 20 Ma. An error analysis is not straightforward, but to the first order, the fourfold differences in cooling rates do not seem consistent with the assumption that the ages of the samples were controlled solely by diffusion-driven losses of ^{40}Ar.

Temperature History for NWA 7034

With results from the previous section, we examine how well the measured Ar/Ar ages of the NWA 7034 samples fit into either of two mathematical descriptions of the time–temperature history of NWA 7034 from 500 °C, the time of sulfidization estimated by Lorand et al. (2015), to closure. One of the descriptions is due to Dodson (1973; equation ii), and the other is the standard result for the cooling of a slab. We will show that neither one accounts for the observations well, which suggests that either the samples did not share a common thermal history or that K gain played an important role in determining the $^{40}Ar/^{39}Ar$ ages.

Dodson's (1973) calculation of closure temperatures assumes that temperature varied with time (t = −1 × age) according to the relation

$$T_j = \left(\frac{1}{T_i} + \frac{R(t_j - t_i)}{E_a \tau}\right)^{-1} \quad (3)$$

where T is temperature in K; R is the gas constant; E_a is again the activation energy; and τ is the e-folding time for the diffusion coefficient. For sample 22350, we have τ = 4.7 Ma based on Equation S6.2 and the ages and activation energies of 22350 and 22346 in Table 8. We may use this information in Equation 3 to predict a temperature of T_j = 500 °C for 22350 when t_j = −1467 Ma. Put another way, these data imply that from the time the samples were at 500 °C, it took 31 Ma for both 22350 and 22346 to cool to the closure temperature of 22350, 239 °C. A similar calculation shows that it took 114 Ma for them to cool further, to the closure temperature of 22346, −5 °C. Figure 8 shows temperature as a function of these elapsed times. Analogous calculations with the results of Table 8 for

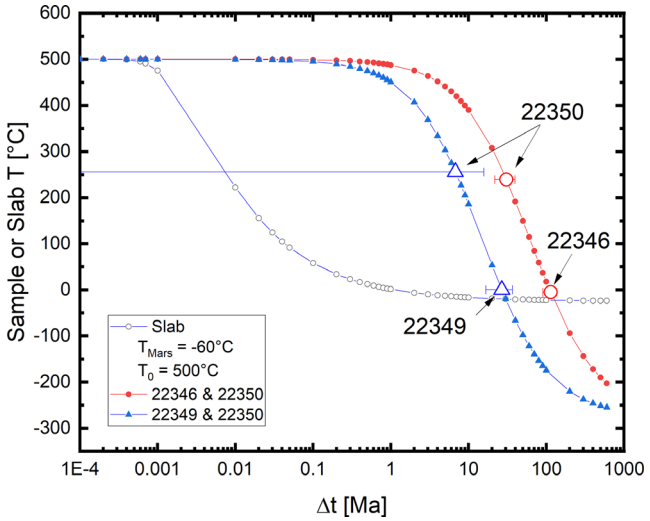

Fig. 8. Test for consistency of measured ages with modeled cooling rates. Sample ages are plotted at calculated closure temperatures (see text). (Color figure can be viewed at wile yonlinelibrary.com.)

the 22350/22349 pair give shorter elapsed times, 7 and 20 Ma, for 22350 and 22349 to reach their respective closure temperatures, 250 °C and 0 °C, from 500 °C. As the elapsed times for the two pairs of samples are inconsistent (Fig. 8), we conclude that Equation 2 does not account for the measured ages.

Figure 8 also shows the time–temperature evolution of the center of a slab of thickness a, and thermal conductivity κ, initially of uniform temperature T_0 = 500 °C, cooled conductively by external material maintained at a temperature T_S, as calculated from the formula of Carslaw and Jaeger (1959).

$$\frac{T - T_S}{T_0 - T_S} = \mathrm{erf}\left(\frac{a}{2\sqrt{\kappa t}}\right) \quad (4)$$

Parameters are given in Table 9. "Initially" (i.e., at T = 500 °C), the slab model yields cooling rates on the order of 10^3 K Ma^{-1}, ~100 times faster than those obtained from Equation 2, a rate so fast that the slab cools to 0 °C, and hence below the likely closure temperatures of all phases, within 1 Ma. Thus, the slab model as parameterized cannot explain the measured age differences between 22350, 22346, and 22349.

In summary, neither the slab model nor Equation 2 accounts well for the apparent differences in ages of samples 22350, 22346, and 22349. One possible explanation is that these age differences are not reliable for technical reasons discussed in Appendix S6. A second possibility that does not exclude the first is that the components of the meteorite had not come together 1.4 Ga BP and therefore did not share a thermal history. Cassata et al. (2018) favor a version of this hypothesis in which the grains were lithified only within the last ~200 Ma. A third possibility is that low-temperature hydrothermal activity reset grain ages, as discussed in the section on a possible connection with nakhlites.

Table 9. Parameters used to model cooling of a slab as in Carslaw and Jaeger (1959).

Thermal conductivity (10^{-6} m^2 s^{-1})[9]	1.00
Slab thickness (km), a	1
Depth of slab top below Mars surface (km)	3
Sample depth below Mars surface (km)	3.5
Initial slab temperature (°C), T_0	500
Surface T (°C)	−60
Geothermal gradient (°C km^{-1})	+10

Notwithstanding the shortcomings of the model calculations, we have one reliable constraint on cooling rates. If temperatures of NWA 7034 reached 500 °C 1.4 Ga ago (e.g., Lorand et al. 2015; McCubbin et al. 2016), then further cooling below 500 °C must have been rapid to preserve the concentration of ^{40}Ar* observed in the samples with rising step release patterns. We estimate a lower bound on the cooling rate from the expression.

$$-(\mathrm{d}T/\mathrm{d}t)|_{T=500^\circ\mathrm{C}} \sim \frac{500^\circ\mathrm{C} - T_2}{\Delta t_{\max}} \geq \frac{\Delta T_{\min}}{\Delta t_{\max}}$$

For T_2 we conservatively adopt 400 °C; use of the closure temperature, ~250 °C, for T_2 would raise the lower bound. Table 8 shows that at 500 °C, it would have taken 22.5 yr for the relatively retentive sample 22345 to lose 90% of the radiogenic ^{40}Ar accumulated between 4.5 and 1.4 Ga, as required by its integrated age. After another 27.9 yr at 500 °C, 22345 would have lost 99% of that radiogenic ^{40}Ar. As a loss of 99% is contrary to observation, we take 27.9 yr to be an upper limit on the time, $\Delta t_{\max}$, that 22345 could have spent at 500 °C. With these choices of $\Delta T_{\min}$ and $\Delta t_{\max}$, we obtain a lower bound of $-(\mathrm{d}T/\mathrm{d}t)|_{T=500^\circ\mathrm{C}} \geq 3.6^\circ\mathrm{C\,yr}^{-1}$. Other samples will have cooled faster. Such rapid cooling appears to be inconsistent with prolonged (>1 Ma) heating at depth.

Timing of ^{4}He Loss

Cassata et al. (2018) argued against helium loss when NWA 7034 was ejected from Mars based on (1) the generally low shock levels recorded in the meteorite; and (2) the observation that nakhlites, despite recording higher shock levels (~5 to 20 GPa; e.g., Fritz et al. 2005) than NWA 7034 (5–15 GPa; Wittmann et al. 2015), retained ^{4}He through launch. The U-Th-Sm/^{4}He age, 50 Ma, of the Light sample suggests that NWA

7034 did lose He and sets an upper limit on the time of loss that is substantially younger than the apparent U/Th/He ages of bulk samples. By itself, this observation does not rule out the preservation of ^{4}He during launch as some loss could have occurred earlier. The observation does require, however, that two unrelated events (a disturbance on Mars followed by launch) took place in a short time. Perhaps more to the point, Dark has an older ^{3}He age than do Light or bulk samples (Table 4). The difference indicates recent helium loss from Light, which is more easily explained either by launch (Schwenzer et al. 2008) in the context of a two-stage CRE history, or by heating thereafter in the context of a one-stage exposure history.

Possible Connections Between the NWA 7034 Clan and Nakhlites/Chassignites

We explore possible launch pairing of the NWA 7034 clan and the nakhlites and chassignites. While the linkage of nakhlites and chassignites is well known (see, e.g., Udry and Day 2018), NWA 7034 bears no strong petrographic relationship to them. NWA 7034 is a polymict breccia that retains a record of formation >4.4 Ga ago; the nakhlites and chassignites are achondrites that crystallized much later. It is the common Martian origin and the timing of major events that occurred from 1.4 Ga on that suggests a connection.

In a recent study of $^{40}Ar/^{39}Ar$ ages, Cohen et al. (2017; their table 1) concluded that nakhlites "sample a layered volcanic sequence with at least four discrete eruptive events spanning 93 ± 12 Ma (1416 ± 7 Ma to 1322 ± 10 Ma [2σ])." This range of ages is consistent with results from other laboratories for nakhlites (Korochantseva et al. [2011] and references therein; Cartwright et al. 2013; Park et al. 2014, 2016) and for Chassigny (Misawa et al. 2006; Korochantseva et al. 2011; and see Udry and Day 2018). The oldest of the $^{40}Ar/^{39}Ar$ ages reported for nakhlites (1418 ± 18 Ma for Nakhla whole rock, Korochantseva et al. [2011] and 1416 ± 7 Ma for Yamato 000749, Cohen et al. [2017]) coincide with the average $^{40}Ar/^{39}Ar$ plateau age of four K-rich grains and one K-poor grain in NWA 7034, 1407 ± 13 Ma (see the Summary of $^{40}Ar/^{39}Ar$ Ages section above).

Cohen et al. (2017; their fig. 3) also presented CRE ages for the six nakhlites analyzed based on measurements of ^{38}Ar. These CRE ages average to 10.7 ± 0.8 Ma (2σ), a value that agrees well with independently obtained averages and measurements for nakhlites and chassignites, for example, 10.9 ± 0.8 Ma ($n = 5$; 2σ mean; Eugster et al. 2006), 11.4 ± 1.0 ($n = 4$; Korochantseva et al. 2011), and 10.8 ± 0.4 Ma ($n = 8$; Herzog and Caffee 2014), and with more recent measurements not included in those averages (Cartwright et al. 2013; Wieler et al. 2016; Park et al. 2016). Recently, Nagao et al. (2016, 2019) reported CRE ages of 11.5 ± 0.7 Ma and 12.3 ± 3.6 Ma for five nakhlites (Nakhla and paired samples MIL 03346, 090030, 090032, 090136) and for three chassignites (Chassigny, NWA 2737, and NWA 8694). These results point strongly, although perhaps not conclusively (see Korochantseva et al. 2011) to a single ejection event for the nakhlites and Chassigny (see also Wieler et al. 2016). As to NWA 7034, our CRE ages for the Dark sample (8–15 Ma) and several of the $^{78,83}Kr$ ages reported by Cassata et al. (2018; 8.3–13.2 Ma) are similar. Other published CRE ages of NWA 7034 for bulk samples are generally younger (Table 4), perhaps because of losses from plagioclase. Although improved values are needed, we think the data allow the assignment of a one-stage CRE age of ~11 Ma.

We examined but found ambiguous two other possible correspondences between the chronologies of NWA 7034 and nakhlites. First, several studies of nakhlites include estimates of the possible times of alteration. Swindle et al. (2000) determined K/Ar ages of weathering products ("iddingsite"), possibly derived from the late alteration of olivine, in Lafayette of 670 ± 91 Ma. As summarized by Borg and Drake (2005; their fig. 4), Shih et al. (1998, 2002) measured Rb/Sr ages of 614–679 Ma in the nakhlites Y000593 and Lafayette and attributed them to alteration. Park et al. (2016) obtained a forced plateau age of 733 ± 38 Ma, perhaps reflecting alteration, for mesostasis from the nakhlite MIL 090030. Two of our NWA 7533 samples, 22239 and 22242, give ages of ~750–800 Ma. These rather uncertain ages appear to be significantly older than the alteration ages of the nakhlites, but the near coincidence is provocative. Second, Korochantseva et al. (2011) noted "a secondary degassing event which affected the K-Ar system of Lafayette mesostasis approximately 1.1 Ga," observing further, "that it may have been a medium-grade long-lasting thermal event (e.g., impact melt sheet covering, late hydrothermal activity) which reset the mesostasis age and did not influence the K-Ar system of magmatic inclusions and the original igneous texture of this rock." This description is close to our conclusions concerning 22239 and 22242.

The hypothesis of launch pairing presumes that the nakhlites, chassignites, and NWA 7034 were in close geographic proximity on Mars (Fig. 9). If so, it takes no great leap of imagination to place NWA 7034 within the thermal sphere of influence of a nakhlite massif, a possibility with several intriguing implications. We consider two modes of possible interaction.

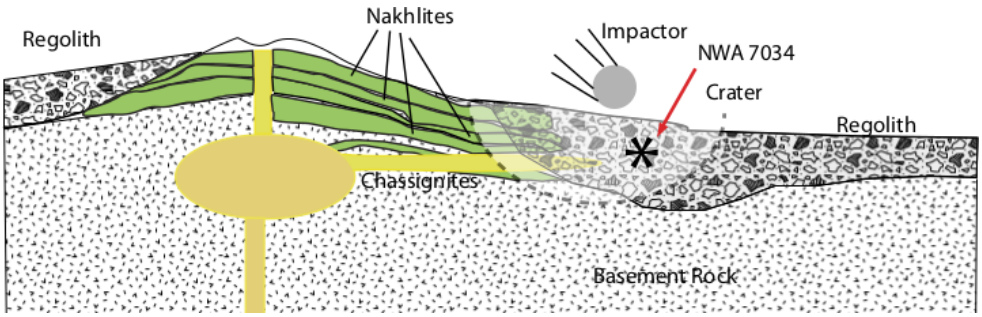

Fig. 9. Possible Martian setting for the nakhlites, chassignites, and NWA 7034 and pairs (not to scale). (Color figure can be viewed at wileyonlinelibrary.com.)

1. As shown schematically in Fig. 9, magmatic/hydrothermal activity associated with nakhlite production 1.4 Ga ago could have heated and sintered proto-NWA 7034 either from below, laterally as drawn in Fig. 9, or from above. Here, we include in "magmatic activity" the production of nearby flows or sills and of hydrothermal fluids that infiltrated the samples (Bridges and Grady 2000; Bridges et al. 2001, 2014). Hydrothermal fluids associated with nakhlites are known to have produced secondary assemblages including Na-K-bearing "gels" and phyllosilicates (Changela and Bridges 2011; Bridges et al. 2014). Such fluids could permeate the adjacent regolith with reactive species and produce secondary mineralization there, too. The observations of MacArthur et al (2019) and Humayun et al. (2019) provide evidence for such processes in the NWA 7034 clan: The former saw K-rich alteration products preserved in porous shocked pyroxene and the latter observed devitrified glass derived from secondary clays. Furthermore, potassium enrichment has been noted in sediments from Gale Crater, suggesting that K-rich brines may be common in Martian sedimentary piles (Fisk et al. 2014).

Prior shock gardening of NWA 7034 components may have enhanced interactions of this kind. Ostertag and Stöffler (1982) demonstrated that shock can cause massive disruption of long-range order in feldspar without any immediate change in composition. When treated with K-rich solution, however, the shocked material will form broad rims enriched in K at laboratory temperatures in a matter of hours or days. The presence of phases especially prone to the loss of ^{40}Ar, that is, of phases with low activation energies in the NWA 7034 breccia, is consistent with the disruption by impact of the feldspar during the pre-nakhlite period.

The potential interchange between a nakhlite massif and the surrounding regolith for a period lasting 50 Ma or more, as inferred for the nakhlites (Cohen et al. 2017), could readily occur and gives ample time for solution-driven recrystallization. We hypothesize that a small portion of an intruding and hot but rapidly cooling hydrothermal fluid enriched in K interacted with proto-NWA 7034 thereby liberating previously accumulated ^{40}Ar and adding K. Given the localized focusing of shock in the breccia, a range of outcomes would be expected from the interactions with hydrothermal fluids. Some feldspar grains may have experienced sufficient shock to permit both thermal resetting and extensive diffusional exchange of K (Ostertag and Stöffler 1982). Milder interactions would result in a spectrum of ^{40}Ar/^{39}Ar ages ranging downward from 4 Ga (Figs. 3 and 5). Clasts that underwent milder interactions with fluids may show partial plateaus with high temperature tails and ages older than 1.4 Ga. The high K clasts may have undergone both more heating by and more extensive exchange of K with the fluid.

In effect, we interpret the ^{40}Ar/^{39}Ar ages of the NWA7034 feldspar clasts analyzed as evidence for a metamorphic aureole around nakhlite/chassignite intrusives and extrusives (Fig. 9). K-rich fluids derived from the hot nakhlite massif drove alteration after earlier impact events had set the stage for Ar loss and K exchange.

2. The heating of NWA 7034 could be a consequence of a separate impact on Mars prior to the one that launched the meteoroids. This scenario would seem to eliminate nakhlites as a source of energy or mass for NWA 7034. An impact close to the nakhlite flows in space and just postdating the oldest of those flows could have caused variable, localized heating of proto-NWA-7034 by hot impact ejecta, and triggered nearby hydrothermal activity as well. Such an impact-driven mechanism requires several coincidences that, all in all, make the impact hypothesis seem less probable than the scenario sketched in (1).

On Concordia plots, numerous zircons in NWA 7034 have lower intercept ages distributed about 1.4 Ga

that are also consistent with a thermal event at this time (Table 1). Metamict zircons that originally crystallized at 4.3 Ga but suffered radiation damage (McCubbin et al 2016) appear to have recrystallized at the same time the feldspars were being partially reset (Nemchin et al. 2014). In addition, Cl-apatite may have been formed by metasomatic fluids (McCubbin et al. 2016) and Re-Os isochrons show disturbances at about the same time (Goderis et al. 2016). Evidence for pyrite recrystallization and siderophile element redistribution require a metasomatic event that is likely to have been coincidental with the 1.4 Ga nakhlite emplacement (Lorand et al. 2015; Goderis et al. 2016). All these observations can be ascribed to a metasomatic episode associated with the nakhlites that took place close to a portion of the Martian regolith that included the NWA clan-to-be.

CONCLUSIONS

$^{40}Ar/^{39}Ar$ data for 16 small (<200 μg) samples are consistent with data obtained for samples 50–5000 times larger (~10 mg; Cassata et al. 2018) and with the small sample analyses of MacArthur et al. (2019). The new data add to the results for the larger samples by confirming prior indications that the ages of K-rich grains tend to cluster near 1.40 Ga, while the step ages of K-poor grains range over more than 2 Ga. Younger $^{40}Ar/^{39}Ar$ ages and/or low activation energies for some components of NWA 7034 may account for the dispersion over 200 Ma of the ages observed for larger, whole-rock samples.

The analytical results for some small samples, for example, the rising temperature release pattern of 22239 (Appendix S3) and the nonlinear Arrhenius plots of 22349 (Fig. 5), show that the argon systematics of microgram masses can be complex. Nonetheless, the $^{40}Ar/^{39}Ar$ ages and thermal parameters measured for NWA 7034 and 7533 samples suggest that a major thermal event or events ~1.40 Ga ago:

- Caused widespread and severe argon loss from most of the components of the meteorite;
- Concluded with partial to complete hydrothermal/diagenetic reworking of K-rich lithologies that may have helped indurate the breccia at low temperature; and
- Lasted no more than 100 Ma, and more likely <50 Ma.

Two low-K samples (22239 and 22342) with distinctly younger step ages, Rb/Sr data from Nyquist et al. (2016), and occasional young step ages in other samples point to some resetting of the argon clock within the last 1.4 Ga. If NWA 7034 was intact, the event(s) must have been mild enough not to disturb the 1.4 Ga step ages observed in other samples. These potentially incompatible requirements may be reconciled for argon by Arrhenius plots showing that the minibulk samples of NWA 7034 (22346 and 22348) contain argon with a remarkably low activation energy, $E_a(^{39}Ar) \sim 100$ kJ mol^{-1}. Generalizing from the results of Weirich et al. (2012) and Sillitoe-Kukas et al (2019), we speculate that this phase was produced when mildly shocked feldspathic material underwent late, highly localized hydrothermal alteration at low temperature with the addition of potassium. Some loss of radiogenic ^4He due to heating could have taken place at the same time.

We cannot rule out, however, either later or earlier lithification of NWA 7034. The evidence from pyrite is open to interpretation (e.g., Hu et al. 2018). And while we have attributed younger ages to what amounts to selective resetting within the intact protometeorite, Cassata et al. (2018) suggested instead that the constituents of NWA 7034 and its pairs came together only within the last ~200 Ma, which would allow grains to have independent histories and a variety of ages. This scenario also readily explains the young, concordant zircon ages of Costa et al. (2020). If lithification occurred late, then temperatures during the process could not have exceeded 250 °C for long without resetting the 1.40 Ga step ages of the K-rich samples. The possibility of very early lithification also remains open (Humayun et al. 2016; Hewins et al. 2017).

A coincidence between the Ar/Ar ages of NWA 7034 samples and those of the nakhlites and chassignites and a permissive though inconclusive coincidence of the CRE ages suggest a linked history from 1.4 Ga through to the time of launch from Mars. We interpret a coincidence in $^{40}Ar/^{39}Ar$ ages at 1.40 Ga as the result of metamorphic/hydrothermal overprinting from a hot nakhlite massif over closely adjacent regolith that included NWA 7034. Variable K enrichment of, and Ar loss from, previously shocked feldspar may account for the range of ages seen among the feldspathic phases, with the degree of resetting dependent on the degree of disorder produced by earlier shock.

Acknowledgments—We thank Dieter Stöffler for instructive comments on the terminology of brecciation, Carl Agee for providing a sample of NWA 7034, and Nicole Lunning for helpful conversation. The manuscript was improved by constructive reviews from Marissa Tremblay and William Cassata and useful advice from Assoc. Editor Marc Caffee. This work was supported in part by NASA Cosmochemistry grant NNX13AL15G (GFH) and NNX16AP98G (MH); Korea Polar Research Institute project PM18030 (KN and JP); and Brain Pool Program through the National

Research Foundation of Korea (NRF) funded by the Ministry of Science and ICT (2018H1D3A2065317) (JP). The authors have no conflict of interest to declare.

Editorial Handling—Dr. Marc Caffee

REFERENCES

Agee C. B., Wilson N. V., McCubbin F., Ziegler K., Polyak V. J., Sharp Z. D., Asmerom Y., Nunn M. H., Shaheen R., Thiemens M. H., Steele A., Fogel M. I., Bowden R., Glamoclija M., Zhang Z., and Elardo S. M. 2013. Unique meteorite from Early Amazonian Mars: Water-rich basaltic breccia Northwest Africa 7034. *Science* 339:780–785.

Atreya S. K., Trainer M. G., Franz H. B., Wong M. H., Manning H. L. K., Malespin C. A., Mahaffy P. R., Conrad P. G., Brunner A. E., Leshin L. A., Jones J. H., Webster C. R., Owen T. C., Pepin R. O., and Navarro-González R. 2013. Primordial argon isotope fractionation in the atmosphere of Mars 1118 measured by the SAM instrument of Curiosity and implications for atmospheric loss. *Geophysical Research Letters* 40:5605–5609. https://doi.org/10.1002/2013GL057763.

Bellucci J. J., Nemchin A. A., Whitehouse M. J., Humayun M., Hewins R., and Zanda B. 2015. Pb-isotopic evidence for an early, enriched crust on Mars. *Earth and Planetary Science Letters* 410:34–41.

Blackburn T., McLean N., and Bowring S. 2017. U-Pb geochronological and thermochronological time-temperature constraints of $^{40}Ar/^{39}Ar$ hornblende reference material HB3gr. *Geostandards & Geoanalytical Research* 41:325–334.

Borg L. and Drake M. J. 2005. A review of meteorite evidence for the timing of magmatism and of surface or near-surface liquid water on Mars. *Journal of Geophysical Research* 110. https://doi.org/10.1029/2005JE002402.

Bouvier L. C., Costa M. M., Connelly J. N., Jensen N. K., Wielandt D., Storey M., Nemchin A. A., Whitehouse M. J., Snapes J. F., Bellucci J. J., Moynier F., Agranier A., Gueguen B., Schönbächler M., and Bizzarro M. 2018. Evidence for extremely rapid magma ocean crystallization and crust formation on Mars. *Nature* 558:586–589.

Bridges J. C. and Grady M. M. 2000. Evaporite mineral assemblages in the nakhlite (Martian) meteorites. *Earth and Planetary Science Letters* 176:267–279.

Bridges J. C., Catling D. C., Saxton J. M., Swindle T. D., Lyon I. C., and Grady M. M. 2001. Alteration assemblages in the Martian meteorites: Implications for near-surface processes. *Space Science Reviews* 96:365–392.

Bridges J. C., Hicks L. J., Hansford G. M., and Gurman S. J. 2014. Martian phyllosilicates in the nakhlite meteorites (abstract #2244). 45th Lunar and Planetary Science Conference. CD-ROM.

Busemann H., Seiler S., Wieler R., Kuga M., Maden C., Irving A. J., Clay P. L., and Joy K. H. 2015. Martian noble gases in recently found shergottites, nakhlites and breccia Northwest Africa 8114 (abstract #5235). 78th Meeting of the Meteoritical Society.

Carslaw H. S. and Jaeger J. C. 1959. *The conduction of heat in solids*, 2nd ed. London: Oxford University Press. 510 p.

Cartwright J. A., Gilmour J. D., and Burgess R. 2013. Martian fluid and Martian weathering signatures identified in Nakhla, NWA 998 and MIL 03346 by halogen and noble gas analysis. *Geochimica et Cosmochimica Acta* 105:255–293.

Cartwright J. A., Ott U., Herrmann S., and Agee C. B. 2014. Modern atmospheric signatures in 4.4 Ga Martian meteorite NWA 7034. *Earth and Planetary Science Letters* 400:77–87.

Cassata W. S. and Borg L. E. 2016. A new approach to cosmogenic corrections in $^{40}Ar/^{39}Ar$ chronometry: Implications for the ages of Martian meteorites. *Geochimica et Cosmochimica Acta* 187:279–293.

Cassata W. S. and Renne P. R. 2013. Systematic variations of argon diffusion in feldspars and implications for thermochronometry. *Geochimica et Cosmochimica Acta* 112:251–287.

Cassata W. S., Cohen B. E., Mark D. F., Trappitsch R., Crow C. A., Wimpenny J., Lee M. R., and Smith C. L. 2018. Chronology of Martian breccia NWA 7034 and the formation of the Martian crustal dichotomy. *Science Advances* 4:eaap8306.

Changela G. and Bridges J. C. 2011. Alteration assemblages in the nakhlites: Variation with depth on Mars. *Meteoritics & Planetary Science* 45:1847–1867.

Cherniak D. J., Watson E. B., and Thomas J. B. 2009. Diffusion of helium in zircon and apatite. *Chemical Geology* 268:155–166.

Cohen B. E., Mark D. F., Cassata W. S., Lee M. R., Tomkinson T., and Smith C. L. 2017. Taking the pulse of Mars via dating of a plume-fed volcano. *Nature Communications* 8. https://doi.org/10.1038/s41467-017-00513-8.

Costa M. M., Jensen N. K., Bouvier L. C., Connelly J. N., Mikouchi T., Horstwood M. S. A., Suuronen J.-P., Moynier F., Deng Z., Agranier A., Martin L. A. J., Johnson T. E., Nemchin A. A., and Bizzarro M. (2020) The internal structure and geodynamics of Mars inferred from a 4.2-Gyr zircon record. *Proceedings of the National Academy of Sciences* 117:30,973–30,979.

Dalrymple G. B., Alexander C. E. Jr., Lanphere M. A., and Kraker G. P. 1981. Irradiation of samples for $^{40}Ar/^{39}Ar$ dating using the Geological Survey TRIGA Reactor. U.S. Geological Survey Professional Paper 1176. pp. 1–55.

Dazé A., Lee J. K. W., and Villeneuve M. 2003. An intercalibration study of the Fish Canyon sanidine and biotite $^{40}Ar/^{39}Ar$ standards and some comments on the age of the Fish Canyon Tuff. *Chemical Geology* 199:111–127.

Dodson M. H. 1973. Closure temperature in cooling geochronological and petrological systems. *Contributions to Mineralogy and Petrology* 40:259–274.

Eugster O. and Michel T. 1995. Common asteroid break-up events of eucrites, diogenites, and howardites and cosmic-ray production rates for noble gases in achondrites. *Geochimica et Cosmochimica Acta* 59:177–199.

Eugster O., Herzog G. F., Marti K., and Caffee M. W. 2006. Recent irradiation and cosmic-ray exposure ages. In *Meteorites and the early solar system II*, edited by Lauretta D. S. and McSween H. Y. Jr. Tucson, Arizona: The University of Arizona Press. pp. 829–851.

Farley K. A. 2002. (U-Th)/He dating: Techniques, calibrations, and applications. *Reviews in Mineralogy and Geochemistry* 47:819–844.

Farley K. A. 2018. Helium diffusion parameters of hematite from a single-diffusion-domain crystal. *Geochimica et Cosmochimica Acta* 231:117–129.

Farley K. A., Malespin C., Mahaffy P., Grotzinger J. P., Vasconcelos P. M., Milliken R. E., Malin M., Edgett K. S., Pavlov A. A., Hurowitz J. A., Grant G. A., Miller H. B., Arvidson R., Beegle L., Calef F., Conrad P. G., Dietrich W. E., Eigenbrode J., Gellert R., Gupta S., Hamilton V., Hassler D. M., Lewis K. W., McLennan S. M., Ming D., Navarro-González R., Schwenzer S. P., Steele A., Stolper E. M., Sumner D. Y., Vaniman D., Vasavada A., Williford K., Wimmer-Schweingruber R. F., and the MSL Science Team. 2014. In situ radiometric and exposure age dating of the Martian surface. *Science* 343:1247166-1-5.

Fechtig H., Gentner W., and Lämmerzahl P. 1963. Argonbestimmungen an Kaliummineralien—XII: Edelgasdiffusionsmessungen an Stein- und Eisenmeteoriten. *Geochimica et Cosmochimica Acta* 27:1149–1169.

Fisk M. R., Dyar M. D., Bridges J., Anderson R. B., Schmidt M. E., Gasnault O., Mangold N., Tokar R. L., Wiens R. C., Gellert R., Blake D. F., Schwenzer S. P., and Edwards P. 2014. Hypotheses on the source of potassium enrichment in some Gale Crater rocks. AGU Fall Meeting 54:08 (abstract).

Fritz J., Greshake A., and Stöffler D. 2005. Micro-Raman spectroscopy of plagioclase and maskelynite in Martian meteorites: Evidence of progressive shock metamorphism. *Antarctic Meteorite Research* 18:96–116.

Garrison D., Hamilin S., and Bogard D. 2000. Chlorine abundances in meteorites. *Meteoritics & Planetary Science* 35:419–429.

Goderis S., Brandon A. D., Mayer B., and Humayun M. 2016. Ancient impactor components preserved and reworked in Martian regolith breccia Northwest Africa 7034. *Geochimica et Cosmochimica Acta* 191:203–215.

Gombosi D. J., Baldwin S. L., Watson E. B., Swindle T. D., Delano J. W., and Roberge W. G. 2015. Argon diffusion in Apollo 16 impact glass spherules: Implications for $^{40}Ar/^{39}Ar$ dating of lunar impact events. *Geochimica et Cosmochimica Acta* 148:251–268.

Guitreau M. and Flahaut J. 2019. Record of low-temperature aqueous alteration of Martian zircon during the late Amazonian. *Nature Communications* 10:2457.

Harrison T. M. and McDougall I. 1982. The thermal significance of potassium feldspar K-Ar ages inferred from $^{40}Ar/^{39}Ar$ age spectrum results. *Geochimica et Cosmochimica Acta* 46:1811–1820.

Harrison T. M., Duncan I., and McDougall I. 1985. Diffusion of ^{40}Ar in biotite: Temperature, pressure and compositional effects. *Geochimica et Cosmochimica Acta* 49:2461–2468.

Harrison T. M., Celerier J., Aikman A. B., Hermann J., and Heizler M. T. 2009. Diffusion of ^{40}Ar in muscovite. *Geochimica et Cosmochimica Acta* 73:1039–1051.

Herzog G. F. and Caffee M. W. 2014. Cosmic-ray exposure ages of meteorites. In *Treatise on Geochemistry*, 2nd ed., Vol. 1, edited by Holland H. D. and Turekian K. K. Oxford: Elsevier. pp. 419–453.

Hewins R. H., Zanda B., Humayun M., Nemchin A., Lorand J.-P., Pont S., Deldicque D., Bellucci J. J., Beck P., Leroux H., Marinova M., Remusat L., Göpel C., Lewin E., Grange M., Kennedy A., and Whitehouse M. J. 2017. Regolith breccia Northwest Africa 7533: Mineralogy and petrology with implications for early Mars. *Meteoritics & Planetary Science* 52:89–124.

Heymann D., Mazor E., and Anders E. 1968. Ages of calcium-rich achondrites I. Eucrites. *Geochimica et Cosmochimica Acta* 32:1241–1268.

Hoffman N. 2001. Modern geothermal gradients on Mars and implications for subsurface liquids (abstract #7044). Conference on the Geophysical Detection of Subsurface Water on Mars, Houston, TX.

Hu J., Liu Y., Asimow P. D., Mai C., Beckett J. R., and Agee C. B. 2018. Unique hydrothermal alteration on mars: Pyrite-polycrystalline pyrrhotite assemblage in Northwest Africa 7034/7533 (abstract #2898). 49th Lunar and Planetary Science Conference. CD-ROM.

Hu S., Lin Y., Zhang J., Hao J., Xing W., Zhang T., Yang W., and Changela H. 2019. Ancient geologic events on Mars revealed by zircons and apatites from the Martian regolith breccia NWA 7034. *Meteoritics & Planetary Science* 54:1–30.

Humayun M., Nemchin A., Zanda B., Hewins R. H., Grange M., Kennedy A., Lorand J.-P., Göpel C., Fieni S., Pont S., and Deldicque D. 2013. Origin and age of the earliest Martian crust from meteorite NWA 7533. *Nature* 503:513–516.

Humayun M., Hidaka H., Yoneda S., Göpel C., Zanda B., and Hewins R. H. 2016. Samarium isotopic constraints for an early compaction age of Northwest Africa 7533 (abstract #1725). 47th Lunar and Planetary Science Conference. CD-ROM.

Humayun M., Sillitoe-Kukas S., Hewins R., Zanda B., Moser D. E., Arcuri G., Irving A. J., and Lorand J.-P. 2019. Spherules in the martian polymict breccias. II. Chemical sedimentary processes on Mars (abstract #2154). 50th Lunar and Planetary Science Conference. CD-ROM.

Jull A. J. T. 2006. Terrestrial ages of meteorites. In *Meteorites and the early solar system II*, edited by Lauretta D. S. and McSween H. Y. Jr. Tucson, Arizona: The University of Arizona Press. pp. 889–905.

Kleine T., Touboul M., Van Orman J. A., Bourdon B., Maden C., Mezger K., and Halliday A. N. 2008. Hf–W thermochronometry: Closure temperature and constraints on the accretion and cooling history of the H chondrite parent body. *Earth and Planetary Science Letters* 270:106–118.

Korochantseva E. V., Schwenzer S. P., Buikin A. I., Hopp J., Ott U., and Trieloff M. 2011. ^{40}Ar-^{39}Ar and cosmic-ray exposure ages of nakhlites—Nakhla, Lafayette, Governador Valadares—and Chassigny. *Meteoritics & Planetary Science* 46:1397–1417.

Kuiper K. F., Deino A., Hilgen F. J., Krijgsman W., Renne P. R., and Wijbrans J. R. 2008. Synchronizing rock clocks of Earth history. *Science* 320:500–504.

Lee J.-Y., Marti K., Severinghaus J. P., Kawamura K., Yoo H.-S., Lee J. B., and Kim J. S. 2006. A redetermination of the isotopic abundances of atmospheric Ar. *Geochimica et Cosmochimica Acta* 70:4507–4512.

Leya I. and Masarik J. 2009. Cosmogenic nuclides in stony meteorites revisited. *Meteoritics & Planetary Science* 44:1061–1086.

Lindsay F., Turrin B., Herzog G. F., Swisher C. III, and Emge T. 2012. $^{39}Ar/^{40}Ar$ ages of single grains from shergottite NWA 2626: Pushing the limits of laser step-heating (abstract #2836). 47th Lunar and Planetary Science Conference. CD-ROM.

Liu Y., Ma C., Beckett J., Chen Y., and Guan Y. 2016. Rare-earth-element minerals in Martian breccia meteorites

NWA 7034 and 7533: Implications for fluid–rock interaction in the Martian crust. *Earth and Planetary Science Letters* 451:251–262.

Lorand J.-P., Hewins R. H., Remusat L., Zanda B., Pont S., Leroux H., Marinova M., Jacob D., Humayun M., Nemchin A., Grange M., Kennedy A., and Göpel C. 2015. Nickeliferous pyrite tracks pervasive hydrothermal alteration in Martian regolith breccia: A study in NWA 7533. *Meteoritics & Planetary Science* 50:2099–2120.

Lorand J.-P., Hewins R. H., Humayun M., Remusat L., Zanda B., La C., and Pont S. 2018. Chalcophile-siderophile element systematics of hydrothermal pyrite from Martian regolith breccia NWA 7533. *Geochimica et Cosmochimica Acta* 241:134–149.

MacArthur J. L., Bridges J. C., Hicks L. J., Burgess R., Joy K. H., Branney M. J., Hansford G. M., Baker S. H., Schwenzer S. P., Gurman S. J., Stephen N. R., Steer E. D., Piercy J. D., and Ireland T. R. 2019. Constraints on the thermal history of Martian regolith breccia Northwest Africa 8114. *Geochimica et Cosmochimica Acta* 246:267–298.

Mahaffy P. R., Webster C. R., Atreya S. K., Franz H., Wong M., Conard P. G., Harpold D., Jones J. H., Leshin L. A., Manning H., Owen T., Pepin R. O., Squyres S., Trainer M., and MSL Science Team. 2013. Abundance and isotopic composition of gases in the Martian atmosphere from the Curiosity 1310 Rover. *Science* 341:263–266.

McCubbin F. M., Boyce J. W., Novák-Szabó T., Santos A. R., Tartèse R., Muttik N., Domokos G., Vazquez J., Keller L. P., Moser D. E., Jerolmack D. J., Shearer C. K., Steele A., Elardo S. M., Rahman Z., Anand M., Delhaye T., and Agee C. B. 2016. Geologic history of Martian regolith breccia Northwest Africa 7034: Evidence for hydrothermal activity and lithologic diversity in the Martian crust. *Journal of Geophysical Research Planets* 121:2120–2149.

McDougall I. and Harrison T. M. 1988. *Geochronology and thermochronology by the $^{40}Ar/^{39}Ar$ method*. New York: Oxford University Press. 212 p.

Min K., Farah A. E., Lee S. R., and Lee J. I. 2017. (U-Th)/He ages of phosphates from Zagami and ALHA77005 Martian meteorites: Implications to shock temperatures. *Geochimica et Cosmochimica Acta* 196:160–178.

Misawa K., Shih C.-Y., Reese Y., Bogard D. D., and Nyquist L. E. 2006. Rb–Sr, Sm–Nd and Ar–Ar isotopic systematics of Martian dunite Chassigny. *Earth and Planetary Science Letters* 246:90–101.

Muttik N., McCubbin F. M., Keller L. P., Santos A. R., McCutcheon W. A., Provencio P. P., Rahman Z., Shearer C. K., Boyce J. W., and Agee C. B. 2014. Inventory of H2O in the ancient Martian regolith from Northwest Africa 7034: The important role of Fe oxides. *Geophysical Research Letters* 41:8235–8244.

Nagao K., Ogata A., Miura Y. N., and Yamaguchi K. 1996. Ar isotope analysis for K-Ar dating using two modified-VG5400 mass spectrometers-I: Isotope dilution method. *Journal of Mass Spectrometry Society of Japan* 44:39–61.

Nagao K., Park J., and Choi H. G. 2008. Noble gases of the Yamato 000027 and Yamato 000097 lherzolitic shergottites from Mars. *Polar Science* 2:195–214.

Nagao K., Haba M. K., Park J., Choi J., Baek J. M., Park C., Lee J. I., Lee M. J., Mikouchi T., Nyquist L. E., Herzog G. F., Turrin B. D., Lindsay F. N., Delaney J. S., and Swisher C. C. III. 2016. Noble gases in Nakhla and three nakhlites Miller Range 090030, 090032, and 090136. 79th Annual Meeting of the Meteoritical Society, 6109 pdf.

Nagao K., Park J., Choi J., Baek J. M., Haba M. K., Mikouchi T., Zolensky M. E., Herzog G. F., Park C., Lee J. I., and Lee M. J. 2019. Genetic relationship between Martian chassignites and nakhlites revealed from noble gases. 82nd Annual Meeting of Meteoritical Society, 6183.pdf.

Nemchin A. A., Humayun M., Whitehouse M. J., Hewins R. H., Lorand J.-P., Kennedy A., Grange M., Zanda B., Fieni C., and Deldicque D. 2014. Record of the ancient martian hydrosphere and atmosphere preserved in zircon from a martian meteorite. *Nature Geoscience* 7:638-642.

Nyquist L. E., Park J., Nagao K., Haba M. K., Mikouchi T., Kusakabe M., Shih C.-Y., and Herzog G. F. 2015 "Normal planetary" Ne-Q in Chelyabinsk and Mars. 78th Mtg. *Meteoritical Society*, 5054.pdf.

Nyquist L. E., Shih C.-Y., McCubbin F. M., Santos A. R., Shearer C. K., Peng Z. X., Burger P. V., and Agee C. 2016. Rb-Sr and Sm-Nd isotopic and REE studies of igneous components in the bulk matrix domain of Martian breccia Northwest Africa 7034. *Meteoritics & Planetary Science* 51:483–498.

Okazaki R. and Nagao K. 2004. Noble gases of Yamato 980459 shergottite. *Antarctic Meteorite Research* 17:68–83.

Ostertag R. and Stöffler D. 1982. Thermal annealing of experimentally shocked feldspar crystals. *Journal of Geophysical Research Supplement* 87:A457–A463.

Palinkaš A. L., Balogh K., Bermanec V., Zebec V. S., and Svingor E. 1996. On use of hyalophane for K-Ar dating in the Central Bosnian Schists Mts. *Acta Geologica Hungarica* 39:149–153.

Park J., Bogard D. D., Nyquist L. E., and Herzog G. F. 2014. Issues in dating young rocks from another planet: Martian shergottites. In *Advances in $^{40}Ar/^{39}Ar$ dating: From archaeology to planetary sciences*, edited by Jourdan F., Mark D., and Verati C. London: Geological Society, Special Publications 378:297–316.

Park J., Herzog G. F., Turrin B. D., Lindsay F. N., Delaney J. S., and Swisher C. C. III. 2016. $^{40}Ar/^{39}Ar$ ages of nakhlites Miller Range (MIL) 090030, 090032 and 090136 (abstract #1821). 47th Lunar and Planetary Science Conference. CD-ROM.

Renne P. R., Balco G., Ludwig K. R., Mundil R., and Min K. 2011. Response to the comment by W.H. Schwarz et al on "Joint determination of 40K decay constants and $^{40}Ar^*/^{40}K$ for the Fish Canyon sanidine standard and improved accuracy for 40Ar/39Ar geochronology" by P.R. Renne et al (2010). *Geochimica et Cosmochimica Acta* 75:5097–5100.

Renne P. R., Mundil R., Balco G., Min K., and Ludwig K. R. 2010. Joint determination of ^{40}K decay constants and $^{40}Ar^*/40K$ for the Fish Canyon sanidine standard, and improved accuracy for $^{40}Ar/^{39}Ar$ geochronology. *Geochimica et Cosmochimica Acta* 74:5349–5367.

Roth A. S. G., Trappitsch R., Metzler K., Hofmann B. A., and Leya I. 2017. Neon produced by solar cosmic 1477 rays in ordinary chondrites. *Meteoritics & Planetary Science* 52:1155–1172.

Schwenzer S. P., Herrmann S., Mohapatra R. K., and Ott U. 2007. Noble gases in mineral separates from three shergottites: Shergotty, Zagami, and EETA79001. *Meteoritics & Planetary Science* 42:387–412.

Schwenzer S. P., Fritz J., Stöffler D., Trieloff M., Amini M., Greshake A., Herrmann S., Herwig K., Jochum K. P., Mohapatra R. K., Stoll B., and Ott U. 2008. Helium loss from Martian meteorites mainly induced by shock metamorphism: Evidence from new data and a literature compilation. *Meteoritics & Planetary Science* 43:1841–1859.

Setera J. B., Turrin B. D., Herzog G. F., VanTongeren J. A., Delaney J. S., and Swisher C. C. III. 2020. $^{40}Ar/^{39}Ar$ thermochronology for submilligram samples using a Ta platform microfurnace, with illustrations from the Bushveld Complex. *Geochemistry Geophysics Geosystems* 21:e2020GC009182.

Shih C.-Y., Nyquist L. E., Reese Y., and Wiesmann H. 1998. The chronology of the nakhlite Lafayette: Rb-Sr and Sm-Nd isotopic ages (abstract #1145). 29th Lunar and Planetary Science Conference. CD-ROM.

Shih C.-Y., Wiesmann H., Nyquist L. E., and Misawa K. 2002. Crystallization age of Antarctic nakhlite Y000593: Further evidence for nakhlite launch pairing. *Antarctic Meteorites* XXVII:151–153.

Sillitoe-Kukas S., Humayun M., Moser D. E., Arcuri G., and Irving A. J. 2019. Hydrothermal infilling of a unique, layered spherule within the martian polymict breccia Northwest Africa 7475 (abstract #2917). 50th Lunar and Planetary Science Conference. CD-ROM.

Steiger R. H. and Jäger E. 1977. Subcommission on geochronology: Convention on the use of decay constants in geo- and cosmochronology. *Earth and Planetary Science Letters* 36:359–362.

Stephenson P. C., Lin Y., and Leya I. 2017. The noble gas concentrations of the Martian meteorites GRV 99027 and paired NWA 7906/NWA 7907. *Meteoritics & Planetary Science* 52:2505–2520.

Stöffler D. and Grieve R. A. F. 2007. Impactites 11, a proposal on behalf of the IUGS Subcommission on the systematics of metamorphic rocks. In *Metamorphic rocks: A classification and glossary of terms, recommendations of the International Union of Geological Sciences*, edited by Fettes D. and Desmons J. Cambridge, UK: Cambridge University Press. pp. 82–92, 111–125.

Swindle T. D., Caffee M. W., and Hohenberg C. M. 1986. Xenon and other noble gases in shergottites. *Geochimica et Cosmochimica Acta* 50:1001–1015.

Swindle T. D., Treiman A. H., Lindstrom D. J., Burkland M. K., Cohen B. A., Grier J. A., Li B., and Olson K. 2000. Noble gases in iddingsite from the Lafayette meteorite: Evidence for liquid water on Mars in the last few hundred million years. *Meteoritics & Planetary Science* 35:107–115.

Tasáryová Z., Fryda J., Janousek V., and Racek M. 2014. Slawsonite–celsian–hyalophane assemblage from a picrite sill (Prague Basin, Czech Republic). *American Mineralogist* 99:2272–2279.

Turner G., Enright M. C., and Cadogan P. H. 1978. The early history of chondrite parent bodies inferred from ^{40}Ar-^{39}Ar ages. Proceedings, 9th Lunar and Planetary Science Conference. pp. 989–1025.

Turrin B. D., Swisher C. C. III, and Deino A. L. 2010. Mass discrimination monitoring and inter-calibration of dual collectors in noble-gas mass spectrometer systems. *Geochemistry, Geophysics, Geosystems* 11. https://doi.org/10.1029/2009GC003013.

Udry A. and Day J. M. D. 2018. 1.34 billion-year-old magmatism on Mars evaluated from the co-genetic nakhlite and chassignite meteorites. *Geochimica et Cosmochimica Acta* 238:292–315.

Vardzelashvili N. S., Omarova M. R., Batyrmurzaev A. S., and Magomedov S. A. 1988. Kinetic parameters of radiogenic argon as sources of geochemical information on metamorphism. *Soobshcheniya Akademii Nauk Gruzinskoi SSR* 129:369–371.

Vermeesch P. 2018. IsoplotR: A free and open toolbox for geochronology. *Geoscience Frontiers* 9:1479–1493.

Weirich J. R., Swindle T. D., Isachsen C. E., Sharp T. G., Li C., and Downs R. T. 2012. Source of potassium in shocked ordinary chondrites. *Geochimica et Cosmochimica Acta* 98:125–139.

Wieler R., Huber L., Busemann H., Seiler S., Leya I., Maden C., Masarik J., Meier M. M. M., Nagao K., Trappitsch R., and Irving A. J. 2016. Noble gases in 18 Martian meteorites and angrite Northwest Africa 7812- Exposure ages, trapped gases, and a re-evaluation of the evidence for solar cosmic ray-produced neon in shergottites and other achondrites. *Meteoritics & Planetary Science* 51:407–428.

Wittmann A., Korotev R. L., Jolliff B. L., Lapen T. J., and Irving A. J. 2014. The petrogenesis of impact basin melt rocks in lunar meteorite Shişr 161. *American Mineralogist* 99:1626–1647.

Wittmann A., Korotev R. L., Jolliff B. L., Irving A. J., Moser D. E., Barker I., and Rumble D. III 2015. Petrography and composition of Martian regolith breccia meteorite Northwest Africa 7475. *Meteoritics & Planetary Science* 50:326–352.

Wordsworth R. D. 2016. The climate of early Mars. *Annual Review of Earth and Planetary Sciences* 44:381–408.

Wotzlaw J.-F., Schaltegger U., Frick D. A., Dungan M. A., Gerdes A., and Günter D. 2013. Tracking the evolution of large-volume silicic magma reservoirs from assembly to supereruption. *Geology* 41:867–870.

Yin Q.-Z., McCubbin F. M., Zhou Q., Santos A. R., Tartèse R., Li X., Li Q., Liu Y., Tang G., Boyce J. W., Lin Y., Yang W., Zhang J., Hao J., Elardo S. M., Shearer C. K., Rowland D. J., Lerche M., and Agee C. B. 2014. An Earth-like beginning for ancient Mars indicated by alkali-rich volcanism at 4.4 Ga (abstract #1320). 45th Lunar and Planetary Science Conference. CD-ROM.

SUPPORTING INFORMATION

Additional supporting information may be found in the online version of this article.

Appendix S1. Cosmogenic He, Ne, and Ar.

Appendix S2. Measured Ar isotope contents of NWA 7533 and NWA 7034 samples.

Appendix S3. Release patterns and isochrons.

Appendix S4. Diffusion parameters calculated from Arrhenius plots.

Appendix S5. Relation between isothermal heating time and the fraction of ^{40}Ar lost.

Appendix S6. Linked calculation of cooling rate and closure temperatures for paired samples.